Hydrological behavior of a deep sub-vertical fault in crystalline basement and relationships with surrounding reservoirs

Clément Roques, Olivier Bour, Luc Aquilina, Benoît Dewandel, Sarah Leray, Jean Michel Schroetter, Laurent Longuevergne, Tanguy Le Borgne, Rebecca Hochreutener, Thierry Labasque, et al.

HYDROLOGICAL BEHAVIOR OF A DEEP SUB-VERTICAL FAULT IN CRYSTALLINE BASEMENT AND RELATIONSHIPS WITH SURROUNDING RESERVOIRS

C. ROQUES*(1), O. BOUR(1), L. AQUILINA(1), B. DEWANDEL(2), S. LERAY(1), JM. SCHROETTER(3), L. LONGUEVERGNE(1), T. LE BORGNE(1), R. HOCHREUTENER(1), T. LABASQUE(1), N. LAVENANT(1), V. VERGNAUD-AYRAUD(1), B. MOUGIN(3)

(1) Université Rennes 1-CNRS, OSUR-Géosciences Rennes, avenue du Général Leclerc, 35000 Rennes, France

(2) BRGM, Water Dept., New Water Resource & Economy Unit, 1039, Rue de Pinville, 34 000 Montpellier, France

(3) BRGM, French Regional Geological Survey of French Brittany, Rennes Atalante Beaulieu 2 rue de Jouanet, 35700 Rennes, France

** Corresponding author: Clément Roques, Université Rennes 1 – CNRS, OSUR Géosciences Rennes, 263 avenue du Général Leclerc, 35000 Rennes, France.*

Email: clement.roques@univ-rennes1.fr

Phone: (0033)2.23.23.54.69.

Fax: (0033)2.23.23.60.90.

ABSTRACT

Crystalline-rock aquifers generally yield limited groundwater resources. However, some highly productive aquifers may be encountered, typically near tectonic discontinuities. In this study, we used a multidisciplinary experimental field approach to investigate the hydrogeological behavior of a sub-vertical permeable fault zone identified by lineament mapping. We particularly focused our investigations on the hydrogeological interactions with neighboring reservoirs.

The geometry of the permeable domains was identified from geological information and hydraulic test interpretations. The system was characterized under natural conditions and during a 9-week large-scale pumping test. We used a combination of piezometric analysis, flow logs, groundwater dating and tracer tests to describe the interactions between permeable domains and the general hydrodynamical behaviors.

A clear vertical compartmentalization and a strong spatial heterogeneity of permeability are highlighted. Under ambient conditions, the vertical permeable fault zone allows discharge of deep groundwater flows within the superficial permeable domain. The estimated flow across the total length of the fault zone ranged from 170 to 200 m^3/day. Under pumping conditions, hydrological data and groundwater dating clearly indicated a flow inversion. The fault zone appears to be highly dependent on the surrounding reservoirs which mainly ensure its recharge. Groundwater fluxes were estimated from tracer tests interpretation. This study demonstrates the hydrogeological capacities of a sub-vertical fault aquifer in a crystalline context. By describing the hydrological behavior of a fault zone, this study provides important constrain about groundwater management and protection of such resources.

Keywords: Hydrogeology, crystalline rocks, lineament, fault zone, large scale pumping test, sustainable groundwater resource.

1 INTRODUCTION

Crystalline rocks cover large areas throughout the world of about 35% of the continental surface (Amiotte Suchet et al., 2003; Blatt and Jones, 1975) and may constitute a crucial water resource for vast population. The porosity and permeability of primary crystalline rocks are extremely low, but their hydraulic properties can be greatly modified as a result of secondary physical processes (unloading, tectonic activities…) and/or geochemical processes such as weathering, fluid circulation (Bahat, 1999; Caine et al., 1996; Evans et al., 1997; Henriksen and Braathen, 2005; Taylor and Howard, 2002, 1999)… Various conceptual models of hydrogeological compartmentalization in crystalline rock aquifers have been proposed (Chilton and Foster, 1995; Dewandel et al., 2006; Maréchal and Wyns, 2004; Taylor and Howard, 1999; Wyns et al., 2004). They usually consist of two main reservoirs: 1) a layer of alterites (<15 meters bgs), identified as a specific reservoir with a relatively high porosity and storage, highly sensitive to rainfall recharge; 2) a superficial fractured zone, of various thickness and which may be characterized by relatively dense sub-horizontal and sub-vertical fracturing. This fractured reservoir has in general a higher permeability although well yields are typically limited to less than 10 m^3/h.

However, highly productive zones have been locally highlighted in regions exposed to past or current tectonic activity, such as Brittany. In practice, although controversial (Gleeson and Novakowski, 2009), hydrogeologists often use fracture outcropping analysis or “lineaments” mapping to determine drilling localization, especially when such lineaments result from extensive tectonic activity (Gleeson and Novakowski, 2009; Henriksen and Braathen, 2005; Sander, 2006; Singhal and Gupta, 2010). Many factors must be considered to ensure the viability of the resource such as rock lithology affected by tectonic activity, stress fields and intensity of deformation. Such factors and fluid flow processes determine fault zone permeability (Caine et al., 1996; Evans et al., 1997; Gleeson and Novakowski, 2009; Goddard and Evans, 1995). Few hydrogeological studies examined relationships between lineaments structures, hydrogeological flow organization and productivity

wells (Fernandes and Rudolph, 2001; Henriksen and Braathen, 2005; Holland and Witthüser, 2011; Richard et al., 2002; Sander, 2006). Fault zones may act as conduits, barriers, or as combined conduit-barrier systems that enhance or impede fluid flow (Bense and Person, 2006; Caine et al., 1996) but can also significantly influence groundwater flow, spring discharge, and water-table elevations (Apaydin, 2010; Gleeson and Novakowski, 2009; Melchiorre et al., 1999).

In some cases, aquifers near highly conductive fault zones and with relatively high production rates for crystalline rocks (from 20 to 100 m^3/h) have been described: Ploemeur aquifer, Brittany (Le Borgne et al., 2006a; Leray et al., 2013; Ruelleu et al., 2010), the New Hampshire Bedrock Aquifer (Richard et al., 2002), Crystalline Rock Aquifers in New England (Harte et al., 2008) and in the Limpopo Province of South Africa (Holland and Witthüser, 2011).

The hydrodynamic functioning of fault structures in various geological contexts has been investigated in several studies. In sedimentary media, Bense et al. (2006; 2003) showed the important effects of the geometry and anisotropy of a fault zone on its hydraulic properties. Numerical studies, such as those by Anderson et al. (Anderson and Bakker, 2008), also highlighted the influence of a vertical fault on groundwater flow. In the crystalline context, some studies have described the permeability architecture and hydrogeological functioning of fault zones for groundwater resources (Boutt et al., 2010; Caine and Tomusiak, 2003; Evans et al., 1997; Ganerod et al., 2008; Stober and Bucher, 1999) or hydrocarbon entrapment (Aydin, 2000). However, very few studies have analyzed the hydrological functioning of faults in a water abstraction context. In this context, aquifer yields will mainly depend on the ability of interactions between the fault and the surrounding reservoirs to allow recharge and water availability. On the other hand, groundwater abstraction from a deep resource will undoubtedly modify the hydrodynamic gradients and lead to mixing between the different reservoirs. The hydrogeological influence of deep fault zones on overlaying reservoirs is poorly known and is apparently difficult to characterize by field studies (Banwart et al., 1994; Carucci et al., 2012; Folch and Mas-Pla, 2008; Gannon et al., 2011; Sophocleous, 2002). This question has been

tackled out only through few numerical studies, which have reported the hydrological efficiency of fault zones to act as preferential flow zone that enhances recharge processes from surrounding reservoirs (Folch and Mas-Pla, 2008; Leray et al., 2013).

The first aim of this study is to characterize the hydrodynamic functioning of a sub-vertical permeable fault zone in crystalline basement from a large-scale field experiment. The main objectives are to i)describe the architecture of the aquifer system, ii) define the flow organization between the permeable zones and recharge processes towards the deep fault zone under natural and pumping conditions and iii) characterize the origin of groundwater and mixing processes due to groundwater abstraction. The experiment is carried out on a specific field site in Brittany (Western France), identified by lineament observation (Carn-Dheilly and Thomas, 2008), where a permeable fault zone at more than 100 meters depth is able to provide about 100 m^3/h according to air-lift flow measurements.

We first describe the characteristics of the groundwater system under ambient conditions to highlight the hydrologic functioning of deep structures at the catchment scale. We then describe a 9-week large-scale pumping test that was carried out to identify the hydraulic properties of the aquifer system. During this test, various complementary experiments and measurements were conducted to investigate flow interactions between the different reservoirs and to identify mixing processes. Finally, the combined analyses from this multidisciplinary experiment are used to develop a hydrogeological conceptual model of a sub-vertical fault zone in crystalline context.

2 GEOLOGICAL AND HYDROGEOLOGICAL SETTING

The experimental site of Saint-Brice en Coglès is located in the Mancellian Domain of the "*Massif Armoricain"*, in Brittany (France), where it constitutes the north western French part of the Cadomian and Variscan orogenies ((Figure 1a). This formation outcrops from western to central Europe and is mainly composed of low to high grade (migmatite) metamorphic rocks, with regional-

117 scale magmatic intrusions (Cadomian granodiorites). The Mancellian Domain is limited in the north
118 by the English Channel, and to the south by the North Armorican Shear Zone (NASZ). The main
119 lithologies encountered are Precambrian (Brioverian) sedimentary rocks ((Figure 1a), composed of
120 alternating series of argillites/siltites and sandstones. These sedimentary rocks have been affected by
121 low grade metamorphism which has formed a metamorphic aureole around the Cadomian
122 granodiorites on a regional-scale (Ballèvre et al., 2009; Brun et al., 2001; Chantraine et al., 2001;
123 Cogné and Wright, 1980). The most important deformation zone corresponds to a major ESE-WNW
124 dextral strike-slip shear zone, the NASZ attributed to hercynian orogeny. Secondary SW-NE reverse
125 faults are also found around this main shear zone. These terrains have been affected by Pyrenean
126 and Alpine orogenies that have generated a diffuse deformation characterized by half-graben basins
127 (Rennes basin, Landéan basin…) and NW-SE sub-vertical faults (Grellet et al., 1993; Van Vliet-Lanoë et
128 al., 1997).

129 The Saint-Brice en Coglès site is located in the epimetamorphism zone of a large Cadomian pluton
130 (Fougère granite). The rocks consist of Brioverian sediments metamorphosed into hornfels schists.
131 The vicinity of the site is characterized by parallel extensional N-S normal faults that form localized
132 extensional basins (Geological map, BRGM (Dadet et al., 1984), (Figure 1b).

133 ***(Figure 1)***

134 Local geological structures were imaged by carrying out a structural analysis including landscape,
135 geological mapping and geophysical (electric and seismic tomographies) analysis. Sub-vertical faults
136 and extensional graben structures were clearly identified ((Figure 2a). In addition, three deep
137 boreholes (MFT20, MFT80 and, F3) were drilled using “Down Hole Air Hammer” drilling method.
138 Another deep borehole (FC4, 250 m), which has been entirely cored, has been drilled along a profile
139 perpendicular to the orientation of the main accident lineament (Figure 2b). The borehole
140 characteristics are detailed in (Table 1. Several shallow boreholes (labeled T in (Figure 2b) were also
141 drilled to characterize the shallow weathered compartment. The first 10 meters contained highly

weathered material with high clay and sand contents. Examination of the cores revealed that the Brioverian rocks were highly deformed and fractured, and intruded by metric aplites, pegmatites and quartz veins, oriented N 50° to N 70°. Particularly, in the vicinity of the fault outcropping, the Brioverian rocks are affected by horizontal fractures, characterized by a density decrease with depth, to an average of about 40-50 meters. The main fault zone was identified in each borehole as a highly fractured and productive zone, ranging from a few meters thick (see core sampling in (Figure 2c) to 15 m in the outcropping part of the borehole ((Table 1 and (Table 2). The fault typically dips by 70° to the NNW ((Figure 2c). Wells were completed with a slotted casing in the deep productive zones.

(Figure 2)

(Table 1)

3 MATERIAL AND METHODS

3.1 FIELD EXPERIMENT

The interactions between the fault zone and the other hydrologic domains were described and quantified by investigating the site under natural conditions and during a large-scale pumping test. A packer was placed 80m below the ground surface in borehole F3 to ensure that pumping was carried out deep within the fault zone. As a result, water abstraction occurred principally from the fault zone at 110 meters below ground surface ((Table 1). Pumping lasted for two months (63 days) at a flow rate of about 45 m^3/h. During the pumping test, total rainfall was limited to 40 mm, and potential evapotranspiration was 90 mm (information available from Saint Mars-sur-la-Futaie weather station- 48°26'N 0°58'W, 30km north-east of the Saint-Brice site). Complementary experiments and analyses carried out are described in the following.

3.2 WATER LEVEL MONITORING AND ANALYSIS

Water levels were recorded using a pressure sensor with barometric compensation (STS© and Schlumberger© pressure transmitters). The altitude of the well was determined by differential GPS. The estimated uncertainty for the absolute water level measurements was about a centimeter. The mean hydraulic parameters of the system under pumping conditions were determined from classic analytical models. In addition, a logarithmic derivative method of drawdown measurement was used to analyze flow regimes (Bourdet and Ayoub, 1989; Renard et al., 2008; Spane and Wurstner, 1993). This method also permitted identification of flow behaviors and an estimation of the system's transmissivity based on Cooper and Jacob's approximation (Renard et al., 2008).

3.3 HIGH RESOLUTION FLOW AND TEMPERATURE LOGGING

Structural heterogeneity of fractured rocks induces flow partitioning within the aquifer system. To examine preferential flow path and fracture connectivity we used high-resolution flow logging (Heat Pulse Flowmeter, Geovista©) under ambient and pumping conditions (Le Borgne et al., 2006b; Paillet, 1998). Single-borehole flowmeter tests provide information on the main inflow or outflow zones in a well and measure the prevailing ambient flow conditions in the absence of pumping (Le Borgne et al., 2006b; Paillet, 1998). During a pumping test, cross-borehole flowmeter tests (pumping in a given well and measurement in another) are based on the observation that transient flow during pumping in a given aquifer modifies the hydraulic head distribution with time in the different permeable domains and produces measurable changes in the vertical flow profiles. The connectivity and hydraulic properties of the main flow paths can be identified by transitory flow measurements (Le Borgne et al., 2006b; Paillet, 1998).

To define flow paths and origin of the water, temperature logging was also used with a multi-parameter Hydrolab probe (OTT©) and Ocean seven 303 CTD (Idronaut©). Differences in hydraulic heads between the fractures in a borehole, under ambient conditions or during pumping, will modify the temperature profile with respect to the geothermic gradient. Therefore these temperature

profiles are very useful to identify hydraulic connections between compartments and their evolution through time (Anderson, 2005; Bense et al., 2008; Chatelier et al., 2011).

3.4 TRACER TESTS

To identify transfer time distribution and to characterize groundwater flows within the main transmissive fault zone, tracer tests were performed between observation wells and the pumped borehole. Tracer breakthrough concentrations were monitored in the pumped well (F3) within the upper casing and below the pump with a flow-through field fluorometer developed by the University of Neuchâtel (Schnegg and Costa, 2007; Schnegg and Flynn, 2002). The fluorometers had been previously calibrated with tracer and local fresh water in the laboratory. To optimize injection, we identified the main fractured part of the fault zone connected to the pumped well (F3) in each observation wells (MFT80 and FC4). Uranine tracer solution was injected in front of the main inflow zone and we checked that no tracer solution remained in the borehole after the injection by logging concentration through borehole depth.

3.5 GEOCHEMISTRY AND GROUNDWATER DATING

To identify water origin and estimate mixing processes, we analyzed geochemistry and groundwater dating data under ambient and pumping conditions. The apparent ages of water samples were determined by measuring Chlorofluorocarbons (CFCs) concentrations. These anthropogenic gases provide information on groundwater resident times up to 50 years and can give information on mixing processes between different water sources during flow changes (Ayraud et al., 2008; Busenberg and Plummer, 1992; Cook and Solomon, 1997; Cook et al., 2005; Jaunat et al., 2012). Waters were sampled in stainless-steel ampoules after discarding at least three ampoule volumes, and ensuring that there was no contact of the water with atmospheric gases.

Groundwater CFCs concentrations were measured by the Geosciences Rennes Laboratory (Labasque, 2006). Water samples were degassed by N2 stripping and then injected into a gas chromatograph

212 equipped with an electron capture detector (GC–ECD). The CFC concentration obtained by
213 chromatographic analysis was converted to the atmospheric mixing ratio (pptv – Parts per Trillion by
214 Volume) by applying a solubility function (modified Henry's Law for trace gases (Ayraud et al., 2008;
215 Bu and Warner, 1995; Warner and Weiss, 1985; Weiss and Price, 1980)). The CFC atmospheric mixing
216 ratios were then compared with the atmospheric evolution curve (Walker et al., 2000) to determine
217 the apparent recharge year, and thus the apparent age of the groundwater. Analytical uncertainty
218 for the CFC concentrations was estimated (Labasque, 2006) at around 3 % for recent water (<20
219 years) and 5 % for old water (between 55 to 30 years).

220 Major and trace elements were analyzed by ion chromatography (Dionex DX-100) and ICP-MS HP
221 4500 at the Geosciences Rennes Laboratory following standard laboratory methods. The analytical
222 uncertainty for major anions and cations was about 2%.

223 4 RESULTS

224 4.1 AMBIENT FLOW CONDITION

225 (Figure 3 shows the evolution of hydraulic head in the main boreholes representative of the
226 fractured domains (FC4, F3, MFT80 and MFT20) and in the upper weathered reservoir (T_i). The
227 seasonal evolution of hydraulic head is similar in all the aquifer system with a fast response to
228 rainfall during the recharge periods and a classic discharge regime observed during summer.

229 The hydraulic head gradient mostly follows the topography and indicates groundwater flow towards
230 the outcropping of the fault zone and discharge into the river (FC4-F3-MFT80 in (Figure 2b&c).
231 Measurements of the hydraulic gradient with depth revealed a higher hydraulic head in the deeper
232 boreholes ((Figure 3). This suggests a definite vertical compartmentalization of the aquifer system.
233 The three boreholes intersecting the permeable fault zone show similar hydraulic responses, with a
234 potential upward flow, according to the hydraulic gradient analysis. The MFT20 well, located at the

edge of the weathered and the fractured bed rock, remains under the influence of the fault zone. The sub-surface aquifer situated within the upper weathered part (T_i boreholes), appears to be much less influenced by the deep structure.

The fault domain responds quickly to rainfall even though it is locally covered by the sub-surface reservoir with lower hydraulic head. This suggests that the bed rock domain can respond rapidly to recharge. The recharge area is certainly along strike and up topographic gradient through favorable deep fractured zones.

(Figure 3)

A typical variation of flow rate with depth is shown in (Figure 4. All flow profiles obtained under ambient conditions reveal upward flow, implying that hydraulic head is higher in the deep fractures (235m for FC4) than in the upper fractures (45m for FC4). FC4 profile in ambient conditions show a major inflow zone at 245 m deep and a major outflow zone at 49 m deep (Figure 4). No other contributing fractures can be detected, either because of the limit of detection of the tool, or simply because of the lack of any hydraulic head gradient between the head in the fractures and the head in the borehole. In pumping conditions, and for a much lower hydraulic head in the borehole, few others fracture may be detected between 160 and 215 meters deep. In any case, the flow rate profiles obtained under pumping conditions confirms that the deep conductive fault zone provides about 50 to 75% of the total productivity of each borehole ((Table 2). For all profiles, the fracture transmissivity was determined by using the model developed by Paillet (1998). The transmissivity of the deep productive sections in each well appeared to be relatively high, ranging between 6 and 9 x 10^{-4} m²/s ((Table 2).

(Table 2)

Groundwater dating by CFCs analyses also highlighted the influence of an old deep water origin, with tracer concentrations close to the detection limit in all deep boreholes ((Table 3), including the 20m

depth well. The apparent water age is older than 55 years. Conversely, CFCs analyses in the first 10 m of the weathered domain revealed recent waters and contamination with nitrate. Globally, the apparent age determined in the upper weathered reservoir and based on a piston flow model, is 20 years. Moreover, the water age in this upper part of the aquifer system decrease uphill. This suggests that the subsurface aquifer is partially influenced by deep groundwater discharge (more or less 25% of old deep water).

(Table 3)

To summarize, three main hydraulic domains were highlighted at the Saint-Brice site: (1) the fault zone which has a higher transmissivity, (2) the surrounding domain affected by secondary fractures less transmissive and (3) the upper weathered part of the aquifer system, restricted to the first 10 meters. Under ambient conditions, the hydrogeological system is clearly driven by the discharge from a deep groundwater system towards the upper part of the aquifer system and the local stream.

(Figure 4)

4.2 PUMPING CONDITION

4.2.1 EVOLUTION OF HYDRAULIC HEADS AND DIAGNOSTIC PLOT

During the 60-days pumping experiment, the hydraulic heads in the different boreholes were recorded ((Figure 5). All wells located in or near the sub-vertical fault zone, including the shallow piezometers in the sub-surface weathered domain, reacted quickly to pumping. During the first 10 days, drawdown was limited to a few meters and was similar in all boreholes. This suggests a good connection between the upper and lower domains of the aquifer system. After 10 days of pumping, drawdown has exceeded the depth of the sub-surface wells (<10 m deep), due to desaturation of the upper weathered reservoir around the pumping well. As observed in all deep boreholes, drawdown increased significantly during the last 50 days of pumping ((Figure 5).

(Figure 5)

283 Figure 6 displays the normalized drawdown (s/Q) of pumping well F3 and its derivative through time
284 in a log-log diagram. The evolution of the derivative curve provides information on flow behaviors
285 and on boreholes effects such as wellbore storage and skyn effects. Such diagnostic curves can be
286 used to interpret different flow regimes (Bourdet et al., 1983; Renard et al., 2008), e.g. double
287 porosity, leakage effect, no-flows boundaries… Here, considering the specific geometry of the aquifer
288 system, we assumed that flow regimes can be described through a simple model developed for
289 fracture or strip aquifer embedded in lower permeable block (Butler and Liu, 1991; Escobar and
290 Hernández, 2010; Gringarten, 1996; Moench, 1984; Rafini and Larocque, 2009; Tiab, 2005). Such
291 fracture models involve generally three characteristic flow regimes: the early local response of the
292 fault zone, a period of transition controlled by the geometrical fault zone properties at larger scale
293 and finally the global hydraulic response of the system.

294 Flow behaviors can be detailed as follow through derivative description: ((Figure 6). 1) After the first
295 early-time where the drawdown response is influenced by wellbore storage and skin effects, a short
296 radial flow response is observed. This reflects the behavior of the local permeable fault zone, where
297 water was principally extracted from the local fracture storage and eventually fed by proximal matrix
298 storage and/or local leakage from overlaying aquifers. The constant derivative value suggests a
299 transmissivity around $10^{-3}\ m^2.s^{-1}$. The derivative decrease between 0.1 and 1 day can be the
300 consequence of preferential leaky flows from shallower reservoir. 2) Between 1 to 30 days of
301 pumping, the drawdown derivative curve is characterized by a transitory period with a strong
302 increase (derivative slope of ½). This derivative increase can be interpreted as double porosity
303 behavior for which lateral inflows from surrounding reservoirs supply the permeable fault at larger
304 scale. The fault geometry can also influence the drawdown during this transitory period which
305 induces linear flow regime. 3) Finally, the system reached a radial flow condition during the last
306 month of pumping, where the whole system was solicited indicating that the major flow comes from
307 surrounding low-permeability domains (Butler and Liu, 1991). The normalized constant derivative of

0.18 m at the end of the test implies a global transmissivity of the aquifer system about $10^{-4}\, m^2.s^{-1}$.

(Figure 6)

4.2.2 FLOWMETER TEST AND TEMPERATURE LOGGING

Flow and temperature logs under natural and pumping conditions are presented for MFT80 in (Figure 7. Other observation wells yielded similar results. Under ambient conditions, upward flows were identified ((Figure 7 a_1), implying that the hydraulic head in the deeper part of the fault zone was higher than in the upper part of the aquifer domain. During pumping, downward flows were measured, indicating a greater decrease of the hydraulic head in the fault zone. Downward flow could be even 3 times greater than the previous upward flow, which implied a clear inversion of flow between the hydraulic permeable domains ((Figure 7 b_1). Nevertheless, the downward borehole flows slowed down after a few days, in conjunction with the decrease in head gradient between the two compartments ((Figure 7 c_1).

Temperature logs ((Figure 7_2), carried out under ambient conditions and during pumping in all observation wells, showed a clear temperature decrease of about 0.2 to 1°C with pumping. The homogeneity of the profiles, with lower temperatures than under ambient conditions, suggests that the deep aquifer domain was fed by colder water coming from the sub-surface domain ((Figure 7 b_2 and c_2). This confirms that pumping is initiated within the fault zone at depth and that the upper aquifer domain is supplying the deeper structure.

(Figure 7)

4.2.3 PUMPING TEST MODELING

The hydraulic parameters of the aquifer system were evaluated by fitting the drawdown data with classic analytical models. Different solutions were applied to interpret the dataset at different times ((Figure 8). in view to characterize the two main flow behaviors involved during the test, previously

characterized by the derivative interpretation: 1) the fault storage response, supported by leaky flow from the weathered part of the aquifer system (<10 days of pumping) and 2) the global double porosity response of the aquifer system during long term pumping.

For the first 10 days of pumping, the double porosity analytical solution according to Moench's model (Moench, 1984) was used to model the local fault zone response. This model is based on the concept of a fracture embedded within blocks of lower permeability, characterized by matrix storage. Solutions are presented in equations 19 and 20 from the Moench paper of 1984 and plotted for the early time in MFT80 for both drawdown and its derivative in (Figure 8a. Quadratic head losses were estimated by a variable rate pumping test at 2.5 10^4 $m^{-5}s^2$. Hydraulic parameters deduced from all wells are listed in (Table 4. These parameters confirm that, during the first days of pumping, flow is controlled by a relatively high transmissive ($T1 = 7.10^{-4} m^2.s^{-1}$) fault zone embedded in lower permeability blocks ($Kb = 2.10^{-8} m.s^{-1}$). A strong fracture skin value (set to 1) was required to model the first times of both drawdown and derivative, which suggest a strong delay contribution between surrounding blocks to the fractured zone (Moench, 1984).

(Table 4)

We also used the "Two Aquifer-System" model developed by Hunt and Scott (2007) to characterize drainage flows from weathered reservoir to the fractured domain. This model assumes a screened well in an aquifer overlain by an aquitard and an unconfined aquifer which may represent here the upper weathered reservoir. A mean transmissivity of $T1 = 5.10^{-4} m^2.s^{-1}$ for the deeper aquifer domain, and transmissivity and porosity estimates of $6.10^{-5} m^2.s^{-1}$ and 2% respectively, for the superficial aquifer was required to fit both drawdowns and derivatives (plot in (Figure 8a, results in (Table 4).

For modeling the hydraulic behavior of the hydrological system at global scale after the first 8 hours of pumping, Moench's model (Moench, 1984) proved to be the simplest and most efficient model to reproduce the data ((Figure 8b). The estimated transmissivity of the fractured system is $T1 =$

$10^{-4}m^2.s^{-1}$, embedded within a reservoir (matrix) with a lower permeability of $Kb = 2.10^{-8}m.s^{-1}$ and a relatively high specific storage of $Sb = 10^{-3}\ m^{-1}$. A high value of fracture skin is still necessary to reproduce the transitory flow regime observed during transitory pumping times (Figure 6). The transmissivity deduced for long times pumping tends to the transmissivity of the global permeable system (Butler and Liu, 1991).

Note that the estimation of storativity in adjacent blocks based on Moench's model is relatively large. However, storativity is in general difficult to estimate in heterogeneous crystalline rocks (Burbey, 2003; Le Borgne et al., 2006a; Meier et al., 1998; Neuman, 1979). This higher value may also reflect the fact that only two main compartments (fracture and matrix) were used in the model, whereas several capacitive domains, including a superficial one in the weathered rocks, may actually be involved in the response to pumping.

(Figure 8)

4.2.4 GEOCHEMISTRY AND GROUNDWATER DATING

Chemical analyses of major ions revealed Ca-Mg-CO_3 in water from the fault zone and Ca-Mg-CO_3 SO_4-Cl, characteristic of anthropogenic activities, in water from the shallower weathered domain. A clear evolution of groundwater chemistry was observed during pumping, due to the mixing of water of different origins. In particular, mixing with the upper weathered reservoir was clearly apparent during the first ten days of pumping. The geochemical response after a longer period was dependent both on shallower and "matrix" contributions and modified by reactivity processes. Description of geochemical evolution will require a much more detailed analysis and will be published in another article (Roques et al., "In Preparation"). Our main focus here is to highlight changes in the apparent age of groundwater, using conservative anthropogenic tracers such as CFCs to highlight the mixing processes.

The evolution of groundwater apparent age was deduced from the CFC-12 and CFC-113 concentrations in samples taken at the pumping wellhead (

(Figure 9). An asymptotic increase in CFCs concentrations was observed, implying a decrease in apparent age, given the assumption of a piston flow model. Under ambient conditions, the CFCs concentrations in the F3 well were negligible, close to the measurement uncertainty, and characteristic of an apparent age exceeding 55 years. After 60 days of pumping, the mean apparent age of water sampled at the outflow was about 40 years. This clearly confirms the influence of the recent water solicited during pumping. Since old water was found in most of the boreholes, this recent water must come from the upper weathered aquifer (<10m). The result also confirms the relatively fast transfer time between compartments.

(Figure 9)

The contribution of the weathered aquifer may easily be estimated by considering a simple binary mixing assumption. We first assumed that mixing occurred between i) water of high apparent age i.e., 55 years (CFC12 concentrations of 0 to 50 pptv) the representative signature of deep fault water, and ii) water from the upper weathered compartment with a mean apparent age of 20 years (CFC12 concentrations of 550 pptv measured in the superficial boreholes before pumping). Based on these assumptions, the estimated contribution of the upper weathered aquifer was around 15-20% at the end of pumping (last 30 days, CFC concentration = 105 pptv).

These observations clearly demonstrate that the superficial compartment contributes to the global mixing process when the deep fault zone aquifer is pumped. It is difficult to clearly define the contribution of each compartment without a detailed analysis of the mixing process (Roques et al., in preparation), which is beyond the scope of the present work. However, both the geochemistry evolution and groundwater dating suggest that after one month of pumping about 20% of the pumped water comes from the upper part of the aquifer system.

4.2.5 TRACER TESTS

Two tracer tests were performed during pumping. Uranine tracer was injected in the main productive fault zone in two observation wells: MFT80 and FC4 at 55 and 235 meters depth respectively. (Figure 10 displays the evolution of normalized concentrations with time for the two breakthrough curves. In the first tracer test (MFT80 towards F3), the tracer was detected 4 hours after injection while the maximum concentration occurred at about 16 hours. The estimated travel distance between the injection point in MFT80 and the main inflow zone in F3 was around 53 meters, implying an average flow velocity of about 3.3 m/h. In the second test (FC4 to F3), the tracer appeared 20 hours after injection and the peak concentration was apparent after about 220h. A slight double peak was observed, certainly due to different flow paths between the two wells. Taking into account a travel distance of about 135m, the estimated average flow velocity in the deep structure was 0.6 m/h, i.e. 5.5 times slower than in the upper part of the fault zone. This implies either that the Darcy velocities were much lower in the deeper compartment or that porosity in the deeper compartment was much higher.

The Becker and Charbeneau (2000) solution for converging radial flow was used to compute the present breackthrough curves (Figure 10). The use of this model is justified for highly dispersive system like this one (Peclet number are around 5, where $Pe = R/\alpha$, with R is the travel distance and α the dispersivity). The modeling objectives are to derive first order transport parameters and to estimate roughly flow partitioning within the permeable fault zone ((Figure 10). The modeling was achieved by setting the injected mass to the restitution rate (around 85% for MFT80 and 45% for FC4). It was not possible to use the same set of parameters to fit the two breakthrough curves ((Figure 10). Firstly, dispersivity was apparently two times higher during the deeper tracer test (FC4). This increase in dispersivity can be explained by a scaling effect that is classically observed in large scale tracer tests (Gelhar, 1992) and due to the integration of heterogeneities along pathways. Secondly, fitting both curves would require either constant flow rates or constant parameters for the fault zone (thickness and porosity). Assuming an average fault thickness of 6 meters and a constant

porosity of around 1 to 2% we were able to obtain a relatively good match for both breackthrough curves ((Figure 10). Porosity values obtained in this case appears relatively high for crystalline rocks, but still reasonable, considering FC4 cores samples (Figure 2), which show that the productive zones are highly fractured and open. The difference in restitution time between the two tracer tests could be honored in this case only by using different effective flowrates for the two tracer tests. This interpretation would imply that the flow-rate from the upper of the aquifer system represented about 2/3 of the total pumping rate while the flow rate from the deeper part was limited to the other 1/3.

Note that the difference in restitution time could be similarly modeled by assuming a permeability decrease with depth or a porosity increase with depth. However, an increase of porosity with depth would be difficult to explain, and permeability, as deduced from previous single borehole tests, appears to remain relatively constant with fault deepening ((Table 2). Such differences may be also partly the results of fault zone heterogeneities. Nevertheless, in both cases tracer injection were done in fractured zone of similar local permeability values. It therefore seems more reasonable to model both tracer tests by assuming flow partitioning through depth.

(Figure 10)

5 DISCUSSION: CONCEPTUAL MODEL

The results obtained in the previous sections were synthesized to derive a global conceptual model of the Saint-Brice en Coglès aquifer system. Our aim was to describe the hydraulic functioning of this steep fault zone under ambient and pumping conditions, and to estimate the groundwater resources actually available.

5.1 SUB-VERTICAL STRUCTURE PROPERTIES AND IMPACT ON GROUNDWATER FLOW

The main permeable structure has developed along an extensive normal fault zone. Boreholes at different depth (MFT80, F3 and FC4) were used to investigate the fault zone properties. The fault permeability appears relatively constant with depth and constitutes a sub-vertical strip fractured zone embedded in low-permeability domains and overlain by a weathered horizontal unconfined domain which does not exceed 10 meters depth (T_i piezometers).

Various complementary approaches were used to characterize the discharge of deep groundwater through the sub-vertical permeable fault zone. Geochemistry and groundwater dating indicated the presence of an old water signature in the fractured domain from 250 to 20m. As the hydraulic heads in the deeper part are higher, the deep water finds a preferential flow path along the permeable fault zone and is discharged towards the subsurface aquifer domains in the watershed outlet (***(Figure 11***a). Fluxes from the deeper part of the aquifer system can be quantified from the fault zone permeability deduced from hydraulic tests and the mean hydraulic gradient between the deep and subsurface domain. Assuming that the flowrate is constant along the length of the fault (about 1000m deduced from the estimated lineament length), the discharge ranges between 170 and 200 m^3/day. Although this amount of natural flux along fault zones is significant, it is generally poorly known, and is not usually considered in the local hydrogeological balance.

(Figure 11)

5.2 FLOW BEHAVIOR AND RELATIONSHIPS BETWEEN COMPARTMENTS UNDER PUMPING CONDITIONS

A multi-disciplinary approach was adopted to investigate flow behavior and water exchanges between the different aquifer domains which enabled us to derive a conceptual model of the hydraulic behavior of this deep permeable fault zone.

The most relevant observation is that the sub-vertical fault is clearly connected with the sub-surface reservoir and the two compartments are therefore highly dependent on each other. Globally, pumping in the deep structure induces downward groundwater flow from the upper aquifer domain (***(Figure 11***b). Due to the limited storage in the fault zone, water fluxes during pumping are mainly supported by the overlaying reservoir and/or adjacent domains. After two months of water extraction, it is clear that pumping involves contributions from the surrounding compartments, which implies sub-surface and lateral inflows (matrix storage) towards the sub-vertical structure. Tracer test analyses showed that about 2/3 of the water flow originates from the upper part of the aquifer system. This partition of fluxes seems to be governed mainly by hydraulic boundary conditions which limit the deep supply during pumping. As a result, the superficial part of the aquifer seems to constitute a key reservoir supplying the faulted bedrock domain during pumping. The lateral influence of pumping seems to be limited to 300 meters from the fault, as observed in some subsurface boreholes. Thus, in the case of a fault with a large dip (approximately 70°) and a high permeability contrast with surrounding compartments, the radial expansion of the drawdown and pressure variation is preferentially transferred along the fault zone. In the present case, pressure variations diffuse mainly along the graben structure, in the lower topographic zone where the wetland has developed (***(Figure 11***b). This behavior implies that fault zones, when they are permeable, may allow pressure diffusion along the fault plane that can act almost as a boundary condition to drain groundwater from the surrounding reservoirs. Similar behavior has been described through numerical modeling of groundwater flow in fault zones (Leray et al., 2013).

CONCLUSIONS

In this study, we used a multidisciplinary approach to investigate the hydrogeologic behavior of a sub-vertical permeable fault and quantify its interactions with surrounding reservoirs, under ambient and pumping conditions. This study provides a good example of the functioning of a sub-vertical fault determined from lineament mapping.

Our results suggest that sub-vertical fault and sub-surface reservoirs are highly dependent on each other. Under ambient conditions, the fault allows the discharge of regional old water into superficial aquifer domains. The natural discharge rate of the fault zone is estimated to be around 170 to 200 m^3/day. Although relatively low, this value should be taken into account when estimating water fluxes, hydrologic budget and solute transport at the watershed scale. During the early stages of pumping, the hydrological system is strongly dependent on storage from the sub-surface weathered reservoir. Once the upper weathered reservoir has become mainly unsaturated, the system acts as a classic dual porosity medium with a highly transmissive structure embedded in lower permeable compartments. Thus, this high permeability fault zone appears to be an efficient thin permeable domain that permits rapid diffusion of pressure but is strongly dependent on sub-surface and adjacent domains of higher storativity. All field measurements suggest that under pumping conditions, most of the flow comes from superficial domains and from the vicinity of the fault zone, with a recharge area located at the surface mainly along the fault zone. Moreover, such steep fault zones, although of relatively high transmissivity, remain relatively limited in terms of groundwater yield. In this study, the pumping test was carried out for 2 months at a flow-rate of 45 m^3/h, but the piezometric analysis indicates that this rate was certainly too high to be sustainable. A better estimate of sustainable flowrate would be around 20 to 30 m^3/h. This is a much lower value than some other fault zone aquifers, such as gently dipping fault zones which may provide higher groundwater resources (Le Borgne et al., 2006a; Ruelleu et al., 2010). This difference confirms the

role of the dip of the fault-zone that may greatly increase borehole yield in some circumstances (Leray et al., 2013).

Acknowledgments

Most funding came from the CASPAR project in collaboration with OSUR and BRGM and co-funded by the French Water Agency of Loire-Brittany (AELB), the Regional of Council of French Brittany, the Department of Ile-et-Vilaine and the French Ministry for Education and Research. We also wish to thank the European Interreg IV project Climawat, which partly funded some of the experiments. We want to thank Matthew Becker and anonymous reviewer for their very constructive and encouraging comments. We would also like to thank Nicolas Guihéneuf for his help to interpret our tracer test results. We thank all the people who were involved in the project: Odile Hénin, Martine Bouhnik-Le Coz, Patrice Petitjean, Patricia Madec, Hélène Pauwels, Flora Lucassou, Jean-Pierre Jegou, Eric Palvadeau, Antoine Armandine Les-Landes, Joaquin Jimenez-Martinez, Pascal Goderniaux, Thomas Stieglitz, Stéphane Durand, Ghislain Ferre, Olivier Dauteil, Christian Camerlynck, Pierre-Yves Galibert, Fayçal Rejiba, Philippe Bardy, Antoine Rivera…

REFERENCES

Amiotte Suchet, P., Probst, J.-L., Ludwig, W., 2003. Worldwide distribution of continental rock lithology: Implications for the atmospheric/soil CO 2 uptake by continental weathering and alkalinity river transport to the oceans. Global Biogeochem. Cycles 17, 1–13.

Anderson, E.I., Bakker, M., 2008. Groundwater flow through anisotropic fault zones in multiaquifer systems. Water Resour. Res. 44, 1–11.

Anderson, M.P., 2005. Heat as a ground water tracer. Ground Water 43, 951–68.

Apaydin, A., 2010. Relation of tectonic structure to groundwater flow in the Beypazari region, NW Anatolia, Turkey. Hydrogeol. J. 18, 1343–1356.

Aydin, A., 2000. Fractures, faults, and hydrocarbon entrapment, migration and flow. Mar. Pet. Geol. 17, 797–814.

Ayraud, V., Aquilina, L., Labasque, T., Pauwels, H., Molenat, J., Pierson-Wickmann, A.-C., Durand, V., Bour, O., Tarits, C., Le Corre, P., 2008. Compartmentalization of physical and chemical properties in hard-rock aquifers deduced from chemical and groundwater age analyses. Appl. Geochemistry 23, 2686–2707.

Bahat, D., 1999. Mechanism of exfoliation joint formation in granitic rocks, Yosemite National Park. J. Struct. Geol. 21, 85–96.

Ballèvre, M., Bosse, V., Ducassou, C., Pitra, P., 2009. Palaeozoic history of the Armorican Massif: Models for the tectonic evolution of the suture zones. Comptes Rendus Geosci. 341, 174–201.

Banwart, S., Gustafsson, E., Laaksoharju, M., 1994. Fracture zone in crystalline bedrock: Initial hydrochemical perturbation during tunnel construction at the Äspö Hard Rock Laboratory, southeastern Sweden. Water Resour. Res. 30, 1747–1763.

Becker, M.W., Charbeneau, R., 2000. First-passage-time transfer functions for groundwater tracer tests conducted in radially convergent flow. J. Contam. Hydrol. 40, 299–310.

Bense, V.F., Person, M. a., 2006. Faults as conduit-barrier systems to fluid flow in siliciclastic sedimentary aquifers. Water Resour. Res. 42, 1–18.

Bense, V.F., Person, M. a., Chaudhary, K., You, Y., Cremer, N., Simon, S., 2008. Thermal anomalies indicate preferential flow along faults in unconsolidated sedimentary aquifers. Geophys. Res. Lett. 35, 1–6.

Bense, V.F., Van den Berg, E.H., Van Balen, R.T., 2003. Deformation mechanisms and hydraulic properties of fault zones in unconsolidated sediments; the Roer Valley Rift System, The Netherlands. Hydrogeol. J. 11, 319–332.

Blatt, H., Jones, R., 1975. Proportions of exposed igneous, metamorphic, and sedimentary rocks. Geol. Soc. Am. Bull. 86, 1085–1088.

571 Bourdet, D., Ayoub, J., 1989. Use of pressure derivative in well test interpretation. SPE
572 Form. Eval. 4, 293–302.

573 Bourdet, D., Whittle, T., Douglas, A., Pirard, Y., 1983. A new set of type curves simplifies well
574 test analysis. World Oil 196, 95–106.

575 Boutt, D.F., Diggins, P., Mabee, S., 2010. A field study (Massachusetts, USA) of the factors
576 controlling the depth of groundwater flow systems in crystalline fractured-rock terrain.
577 Hydrogeol. J. 18, 1839–1854.

578 Brun, J.-P., Guennoc, P., Truffert, C., Vairon, J., 2001. Cadomian tectonics in northern
579 Brittany: a contribution of 3-D crustal-scale modelling. Tectonophysics 331, 229–246.

580 Bu, X., Warner, M.J., 1995. Solubility of chlorofluorocarbon 113 in water and seawater. Deep
581 Sea Res. Part I Oceanogr. Res. Pap. 42, 1151–1161.

582 Burbey, T.., 2003. Use of time–subsidence data during pumping to characterize specific
583 storage and hydraulic conductivity of semi-confining units. J. Hydrol. 281, 3–22.

584 Busenberg, E., Plummer, L.N., 1992. Use of chlorofluorocarbons (CCl3F and CCl F2) as
585 hydrologic tracers and age-dating tools: The alluvium and terrace system of central
586 Oklahoma. Water Resour. Res. 28, 2257–2283.

587 Butler, J.J., Liu, W.Z., 1991. Pumping tests in non-uniform aquifers: the linear strip case. J.
588 Hydrol. 128, 69–99.

589 Caine, J., Evans, J., Forster, C., 1996. Fault zone architecture and permeability structure.
590 Geology 24, 1025–1028.

591 Caine, J.S., Tomusiak, S.R.A., 2003. Brittle structures and their role in controlling porosity
592 and permeability in a complex Precambrian crystalline-rock aquifer system in the
593 Colorado Rocky Mountain Front Range. GSA Bull. 115, 1410–1424.

594 Carn-Dheilly, A., Thomas, E., 2008. RAPSODI - Recherche d'aquifères profonds dans le
595 socle du département de l'Ille et Vilaine. Rapport Final - BRGM/RP-56749-FR.

596 Carucci, V., Petitta, M., Aravena, R., 2012. Interaction between shallow and deep aquifers in
597 the Tivoli Plain (Central Italy) enhanced by groundwater extraction: A multi-isotope
598 approach and geochemical modeling. Appl. Geochemistry 27, 266–280.

599 Chantraine, J., Egal, E., Thiéblemont, D., Le Goff, E., Guerrot, C., Ballèvre, M., Guennoc, P.,
600 2001. The Cadomian active margin (North Armorican Massif, France): a segment of the
601 North Atlantic Panafrican belt. Tectonophysics 331, 1–18.

602 Chatelier, M., Ruelleu, S., Bour, O., Porel, G., Delay, F., 2011. Combined fluid temperature
603 and flow logging for the characterization of hydraulic structure in a fractured karst
604 aquifer. J. Hydrol. 400, 377–386.

605 Chilton, P.J., Foster, S.D.S., 1995. Hydrogeological characterization and water-supply
606 potential of basement aquifers in tropical Africa. Hydrogeol. J. 3, 36–49.

607 Cogné, J., Wright, A.E., 1980. L'orogène Cadomien – Geology of Europe from Precambrian
608 to the post-Hercynian sedimentary basins. 26th Int. Geol. Congr. – BRGM Mem 108,
609 29–55.

610 Cook, P., Love, a, Robinson, N., Simmons, C., 2005. Groundwater ages in fractured rock
611 aquifers. J. Hydrol. 308, 284–301.

612 Cook, P., Solomon, D., 1997. Recent advances in dating young groundwater:
613 chlorofluorocarbons, 3H/3He and 85Kr. J. Hydrol. 191, 245–265.

614 Dadet, P., Beurrier, M., Lautridou, J.-P., 1984. Notice explicative de la feuille Saint-Hilaire-
615 Du-Harcouët à 1/50 000. BRGM, Orléans.

616 Dewandel, B., Lachassagne, P., Wyns, R., Maréchal, J.C., Krishnamurthy, N.S., 2006. A
617 generalized 3-D geological and hydrogeological conceptual model of granite aquifers
618 controlled by single or multiphase weathering. J. Hydrol. 330, 260–284.

619 Escobar, F.H., Hernández, D.P., 2010. Pressure and pressure derivative analysis for long
620 naturally fractured reservoirs using the TDS technique. DYNA 77, 102–114.

621 Evans, J.P., Forster, C.B., Goddard, J. V., 1997. Permeability of fault-related rocks, and
622 implications for hydraulic structure of fault zones. J. Struct. Geol. 19, 1393–1404.

623 Fernandes, A., Rudolph, D., 2001. The influence of Cenozoic tectonics on the groundwater-
624 production capacity of fractured zones: a case study in Sao Paulo, Brazil. Hydrogeol. J.
625 9, 151–167.

626 Folch, A., Mas-Pla, J., 2008. Hydrogeological interactions between fault zones and alluvial
627 aquifers in regional flow systems. Hydrol. Process. 22, 3476–3487.

628 Ganerod, G.V., Braathen, A., Willemoes-Wissing, B., 2008. Predictive permeability model of
629 extensional faults in crystalline and metamorphic rocks; verification by pre-grouting in
630 two sub-sea tunnels, Norway. J. Struct. Geol. 30, 993–1004.

631 Gannon, J.P., Burbey, T.J., Bodnar, R.J., Aylor, J., 2011. Geophysical and geochemical
632 characterization of the groundwater system and the role of Chatham Fault in
633 groundwater movement at the Coles Hill uranium deposit, Virginia, USA. Hydrogeol. J.
634 20, 45–60.

635 Gelhar, L., 1992. A critical review of data on field-scale dispersion in aquifers. Water Resour.
636 Res. 28, 1955–1974.

637 Gleeson, T., Novakowski, K., 2009. Identifying watershed-scale barriers to groundwater flow:
638 Lineaments in the Canadian Shield. Geol. Soc. Am. Bull. 121, 333–347.

639 Goddard, J. V., Evans, J.P., 1995. Chemical changes and fluid-rock interaction in faults of
640 crystalline thrust sheets, northwestern Wyoming, U.S.A. J. Struct. Geol. 17, 533–547.

641 Grellet, B., Combes, P., Granier, T., Philip, H., 1993. Sismotectonique de la France
642 métropolitaine dans son cadre géologique et géophysique. Mem. N.S. SGF 164 1-2.

643 Gringarten, E., 1996. 3-D geometric description of fractured reservoirs. Math. Geol. 28, 881–
644 893.

645 Harte, P., Robinson, G., Ayotte, J., Flanagan, S., 2008. Framework for Evaluating Water
646 Quality of the New England Crystalline Rock Aquifers. U.S. Geol. Surv. Open-File Rep.
647 2008–1282 47.

648 Henriksen, H., Braathen, A., 2005. Effects of fracture lineaments and in-situ rock stresses on
649 groundwater flow in hard rocks: a case study from Sunnfjord, western Norway.
650 Hydrogeol. J. 14, 444–461.

651 Holland, M., Witthüser, K.T., 2011. Evaluation of geologic and geomorphologic influences on
652 borehole productivity in crystalline bedrock aquifers of Limpopo Province, South Africa.
653 Hydrogeol. J. 19, 1065–1083.

654 Hunt, B., Scott, D., 2007. Flow to a Well in a Two-Aquifer System. J. Hydrol. Eng. 12, 146–
655 155.

656 Jaunat, J., Huneau, F., Dupuy, A., Celle-Jeanton, H., Vergnaud-Ayraud, V., Aquilina, L.,
657 Labasque, T., Le Coustumer, P., 2012. Hydrochemical data and groundwater dating to
658 infer differential flowpaths through weathered profiles of a fractured aquifer. Appl.
659 Geochemistry 27, 2053–2067.

660 Labasque, T., 2006. Analyse des CFC dans les eaux souterraines. Géosciences Rennes,
661 Cahiers techniques de Géosciences Rennes, Rennes.

662 Le Borgne, T., Bour, O., Paillet, F., Caudal, J., 2006a. Assessment of preferential flow path
663 connectivity and hydraulic properties at single-borehole and cross-borehole scales in a
664 fractured aquifer. J. Hydrol. 328, 347–359.

665 Le Borgne, T., Paillet, F., Bour, O., Caudal, J.-P., 2006b. Cross-borehole flowmeter tests for
666 transient heads in heterogeneous aquifers. Ground Water 44, 444–52.

667 Leray, S., de Dreuzy, J.-R., Bour, O., Bresciani, E., 2013. Numerical modeling of the
668 productivity of vertical to shallowly dipping fractured zones in crystalline rocks. J. Hydrol.
669 481, 64–75.

670 Maréchal, J., Wyns, R., 2004. Vertical anisotropy of hydraulic conductivity in the fissured
671 layer of hard-rock aquifers due to the geological structure of weathering profiles. J.
672 Geol. Soc. India 5, 545–550.

673 Meier, P.M., Carrera, J., Sánchez-Vila, X., 1998. An evaluation of Jacob's Method for the
674 interpretation of pumping tests in heterogeneous formations. Water Resour. Res. 34,
675 1011–1025.

676 Melchiorre, E.B., Criss, R.E., Davisson, M.L., 1999. Relationship between seismicity and
677 subsurface fluids, central Coast Ranges, California. J. Geophys. Res. 104, 921–939.

678 Moench, F., 1984. Double-Porosity Models for a Fissured Groundwater Reservoir With
679 Fracture Skin. Water Ressources Res. 20, 831–846.

680 Neuman, S.P., 1979. Perspective on "Delayed yield". Water Resour. Res. 15, 899–908.

681 Paillet, F.L., 1998. Flow modeling and permeability estimation using borehole flow logs in
682 heterogeneous fractured formations. Water Resour. Res. 34, 997–1010.

683 Rafini, S., Larocque, M., 2009. Insights from numerical modeling on the hydrodynamics of
684 non-radial flow in faulted media. Adv. Water Resour. 32, 1170–1179.

685 Renard, P., Glenz, D., Mejias, M., 2008. Understanding diagnostic plots for well-test
686 interpretation. Hydrogeol. J. 17, 589–600.

687 Richard, B., Moore, B., Schwarz, G.E., Clark, S.F., Walsh, G.J., Degnan, J.R., 2002. Factors
688 Related to Well Yield in the Fractured-Bedrock Aquifer of New Hampshire. U.S. Geol.
689 Surv. Prof. Pap. 1660, 1–51.

690 Ruelleu, S., Moreau, F., Bour, O., Gapais, D., Martelet, G., 2010. Impact of gently dipping
691 discontinuities on basement aquifer recharge: An example from Ploemeur (Brittany,
692 France). J. Appl. Geophys. 70, 161–168.

693 Sander, P., 2006. Lineaments in groundwater exploration: a review of applications and
694 limitations. Hydrogeol. J. 15, 71–74.

695 Schnegg, P., Costa, R., 2007. Tracer tests made easier with field fluorometers. Bull.
696 d'Hydrogéologie 20, 20–21.

697 Schnegg, P., Flynn, R., 2002. Online field fluorometers for hydrogeological tracer tests. Isot.
698 und Tracer der Wasserforschung, Tech. Univ. Bergakademie Freiberg,
699 Wissenschaftliche Mitteilungen, Inst. für Geol. 19, 29–36.

700 Singhal, B., Gupta, R., 2010. Applied Hydrogeology of Fractured Rocks: Second Edition.
701 Springer.

702 Sophocleous, M., 2002. Interactions between groundwater and surface water: the state of
703 the science. Hydrogeol. J. 10, 52–67.

704 Spane, F., Wurstner, S., 1993. DERIV: A computer program for calculating pressure
705 derivatives for use in hydraulic test analysis. Ground Water 31, 814–822.

706 Stober, I., Bucher, K., 1999. Deep groundwater in the crystalline basement of the Black
707 Forest region. Appl. Geochemistry 14, 237–254.

708 Taylor, R., Howard, K., 2002. A tectono-geomorphic model of the hydrogeology of deeply
709 weathered crystalline rock: Evidence from Uganda. Hydrogeol. J. 8, 279–294.

710 Taylor, R.G., Howard, K.W.F., 1999. Lithological evidence for the evolution of weathered
711 mantles in Uganda by tectonically controlled cycles of deep weathering and stripping.
712 CATENA 35, 65–94.

713 Tiab, D., 2005. Analysis of pressure derivative data of hydraulically fractured wells by the
714 Tiab's Direct Synthesis technique. J. Pet. Sci. Eng. 49, 1–21.

715 Van Vliet-Lanoë, B., Bonnet, S., Hallegouët, M., Laurent, M., 1997. Neotectonic and seismic
716 activity in the Armorican and Cornubian Massifs: Regional stress field with glacio-
717 isostatic influence? J. Geodyn. 24, 219–239.

718 Walker, S.J., Weiss, R.F., Salameh, P.K., 2000. Reconstructed histories of the annual mean
719 atmospheric mole fractions for the halocarbons CFC-11 CFC-12, CFC-113, and carbon
720 tetrachloride. J. Geophys. Res. 105, 14285.

721 Warner, M.J., Weiss, R.F., 1985. Solubilities of chlorofluorocarbons 11 and 12 in water and
722 seawater. Deep Sea Res. Part A. Oceanogr. Res. Pap. 32, 1485–1497.

723 Weiss, R.F., Price, B.A., 1980. Nitrous oxide solubility in water and seawater. Mar. Chem. 8,
724 347–359.

725 Wyns, R., Baltassat, J., Lachassagne, P., Legchenko, A., Vairon, J., 2004. Application of
726 proton magnetic resonance soundings to groundwater reserve mapping in weathered
727 basement rocks (Brittany, France). Bull. la Société Géologique Fr. 175, 21–34.

728

Figure captions

Figure 1: a) Location map and regional geological map. Star symbol indicates the St Brice Field site, 48°25'N 1°22'W, alt. 90m a.s.l. (modified from Chantraine, (Chantraine et al., 2001)*). b) Local geological map with main lineaments identified (modified Dadet,* (Dadet et al., 1984) *& IGN©).*

Figure 2: Geological conceptual model of the St Brice field site. a) Conceptual geological structure in a 3D diagram representation, b) local geological map and boreholes location and c) cross-section of the structure perpendicular to the main identified lineament.

Figure 3 : Typical hydraulic head variations measured in the different boreholes at Saint-Brice and precipitations measured during the same period. Rainfall was measured at the nearest meteorological station located 30 kilometers from Saint-Brice.

Figure 4: Flowrate profiles in FC4 borehole under (a) ambient conditions (before pumping), measured with a Heat-Pulse-Flowmeter, and (b) pumping conditions, measured with an Impeller Flowmeter Geovista©. The blue straight line represents the modeled flow using Paillet solutions (Paillet, 1998).

Figure 5 : Drawdown in the pumping well (F3, blue triangle dots), in observation wells intersecting the fault zone aquifer (FC4, MFT80 and MFT20, gray points) and observation wells located in the shallow aquifer (T1, T2, T3, T5, T6 and T7, black lines)

Figure 6 : Diagnostic plot in Log scales showing drawdown (blue straight line) normalized by flow rate (s/Q), and its derivative (blue point symbol) measured during the long term pumping test in F3.

Figure 7: Flow and temperature profiles under ambient (grey lines) and pumping conditions (after 9 and 63 days of pumping) in observation well (MFT80).

Figure 8 : Drawdown (s) evolution with time and its derivative (s') during pumping. Observations come from MFT80 observation well. Moench and Boulton (modified Hunt) analytical models were used to fit both drawdown and derivative curves. In a) only the first ten days were fitted while in b) Moench's model was fitted to pumping results obtained at later times.

Figure 9 : Apparent age of water sampled at the outflow and deduced from CFC analysis.

Figure 10 : Tracer test data between the shallow aquifer (MFT80, gray point symbol) and the deep fracture (FC4, gray triangle symbol), modeled with the Welty and Gelhar solution (gray straight lines). Parameters used in the model are presented in the table (Welty and Gelhar, 1994).

Figure 11 : Conceptual model of groundwater flow at the St-Brice site under a) ambient conditions and b) pumping conditions

Table 1: Borehole descriptions

Table 2: Transmissivity results obtained by modeling borehole flow profiles using Paillet solutions (Paillet, 1998).

Table 3: CFC and SF6 concentrations converted into atmospheric concentration (PPTV, (Bu and Mark J Warner, 1995; M.J. Warner and Weiss, 1985)).

Table 4: Pumping test results for pumping well F3 and observation wells MFT80, FC4 and MFT20. RMSE is calculated over the analyzed part of the pumping test.

FIG1.pdf

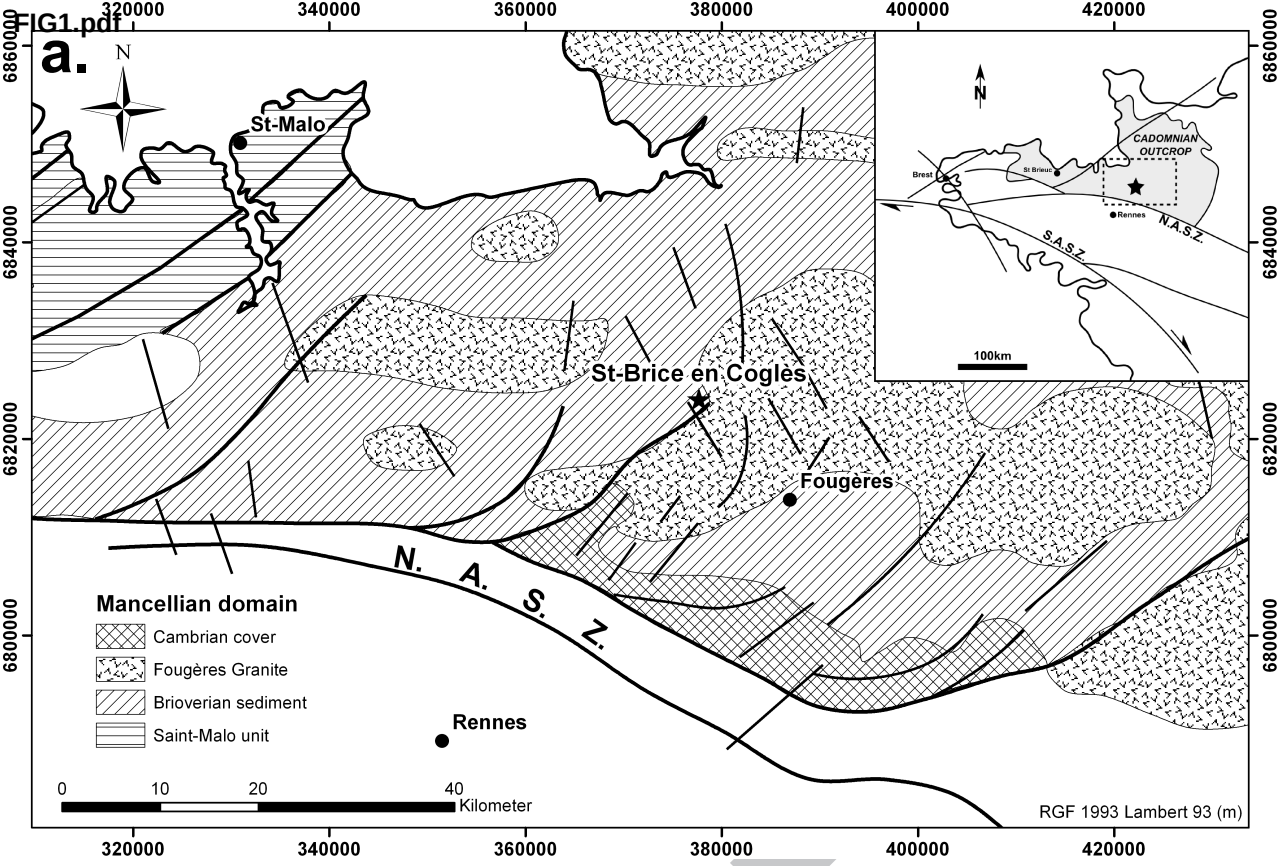
a.
N
St-Malo
St-Brice en Coglès
Fougères
Rennes
N. A. S. Z.
Mancellian domain
Cambrian cover
Fougères Granite
Brioverian sediment
Saint-Malo unit
0 10 20 40 Kilometer
RGF 1993 Lambert 93 (m)
320000 340000 360000 380000 400000 420000
6860000 6840000 6820000 6800000
CADOMNIAN OUTCROP
Brest
St Brieuc
Rennes
S.A.S.Z.
N.A.S.Z.
100km

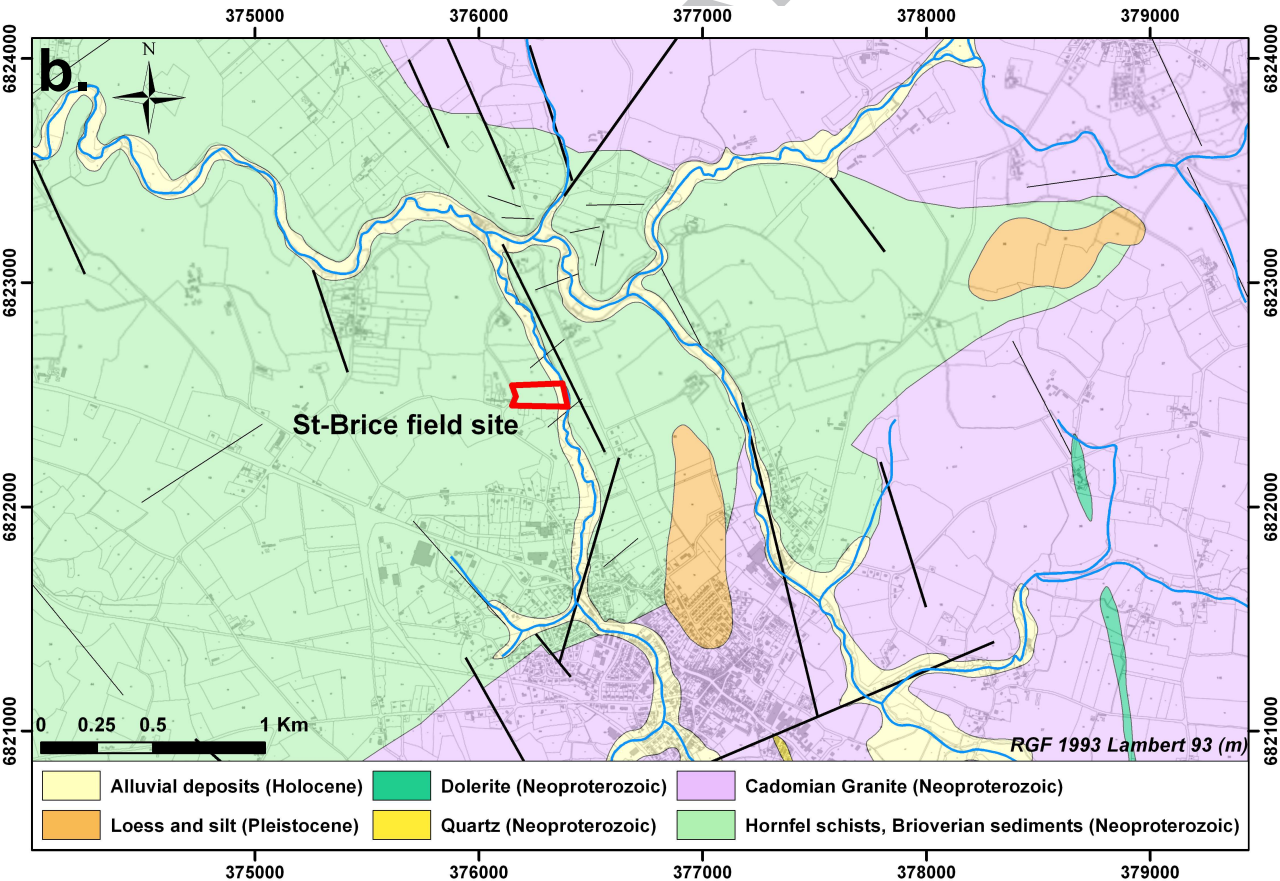
b.
N
St-Brice field site
0 0.25 0.5 1 Km
RGF 1993 Lambert 93 (m)
375000 376000 377000 378000 379000
6824000 6823000 6822000 6821000
Alluvial deposits (Holocene)
Loess and silt (Pleistocene)
Dolerite (Neoproterozoic)
Quartz (Neoproterozoic)
Cadomian Granite (Neoproterozoic)
Hornfel schists, Brioverian sediments (Neoproterozoic)

Figure

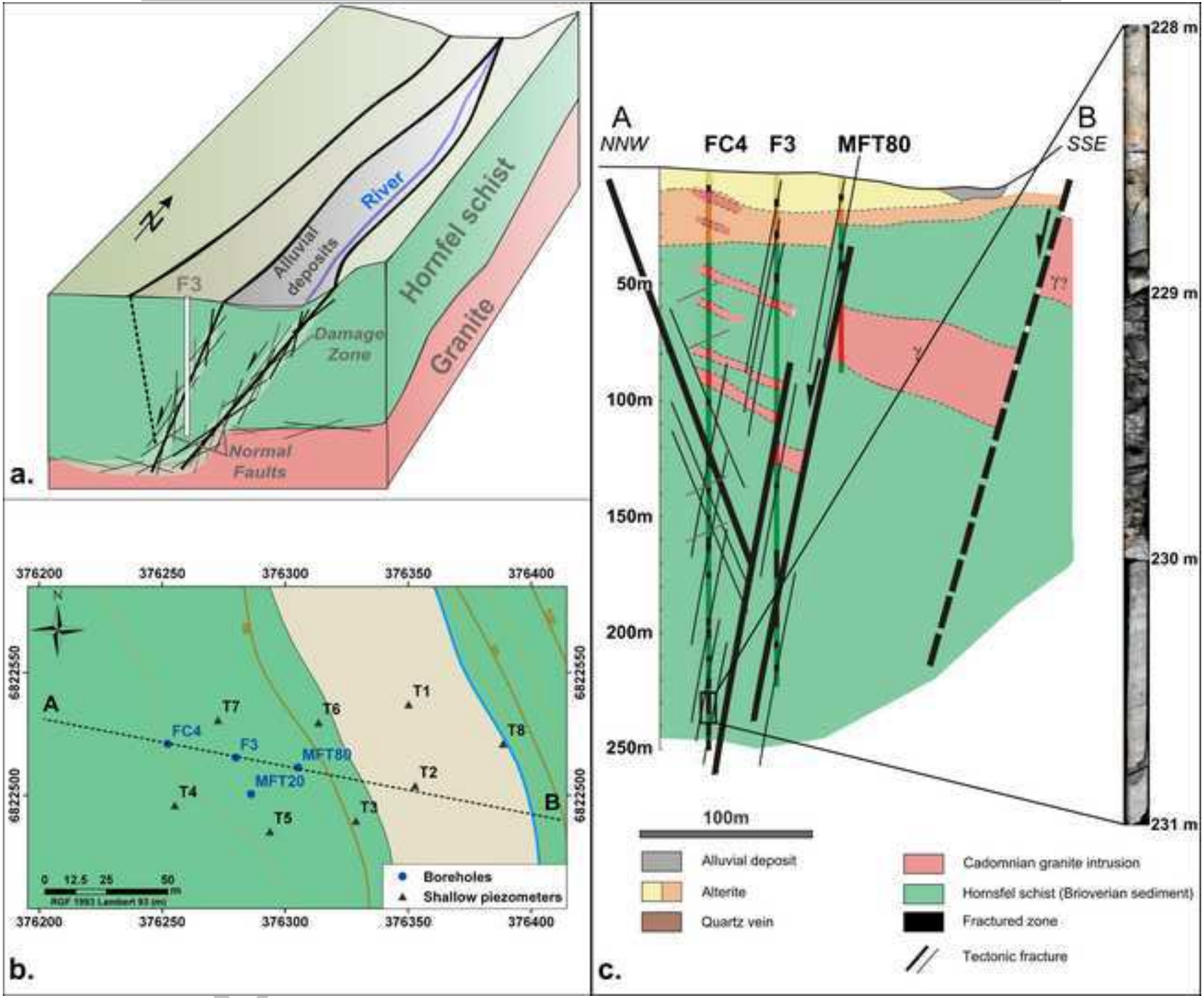

Figure

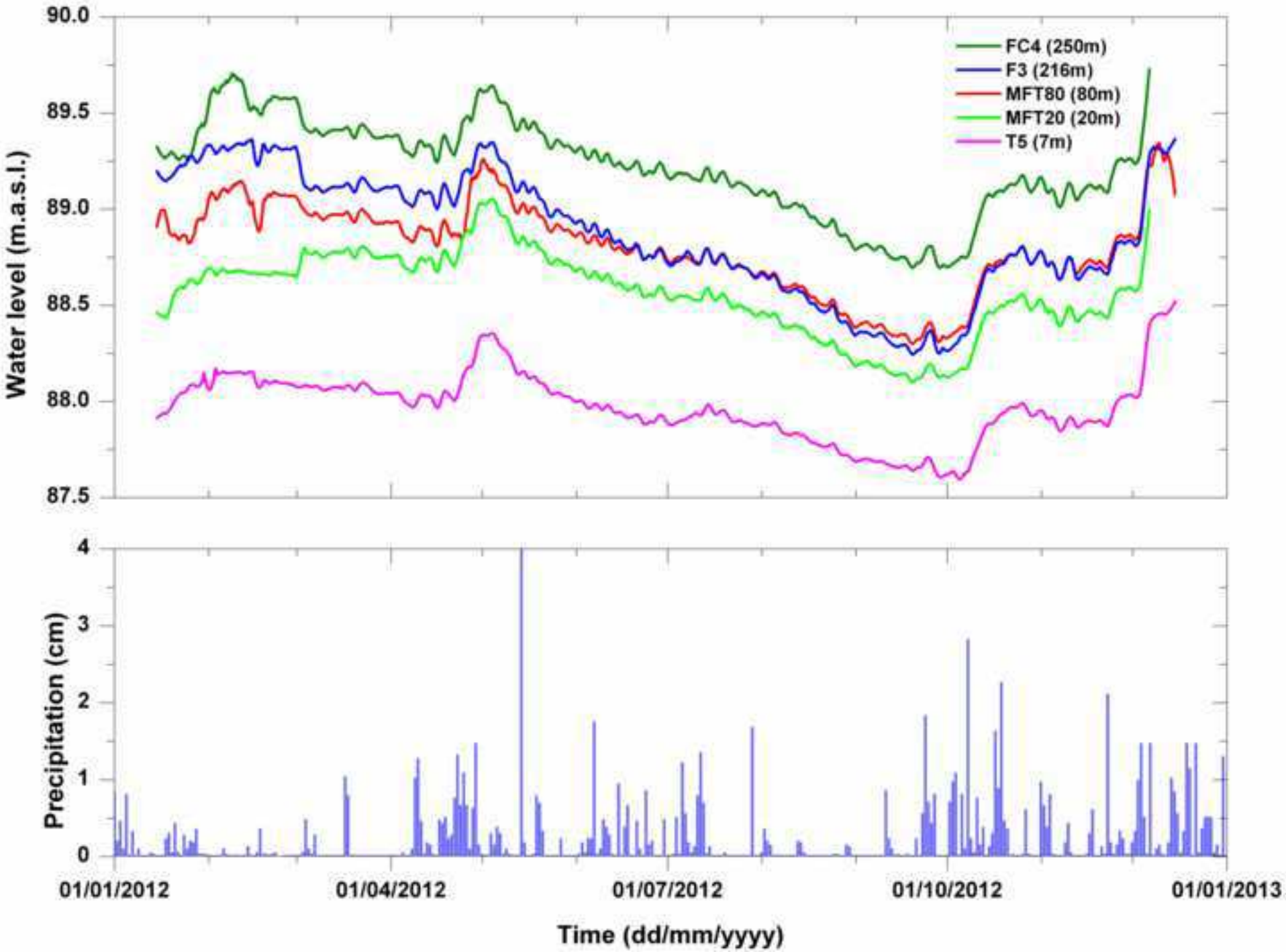

FIG4.tif

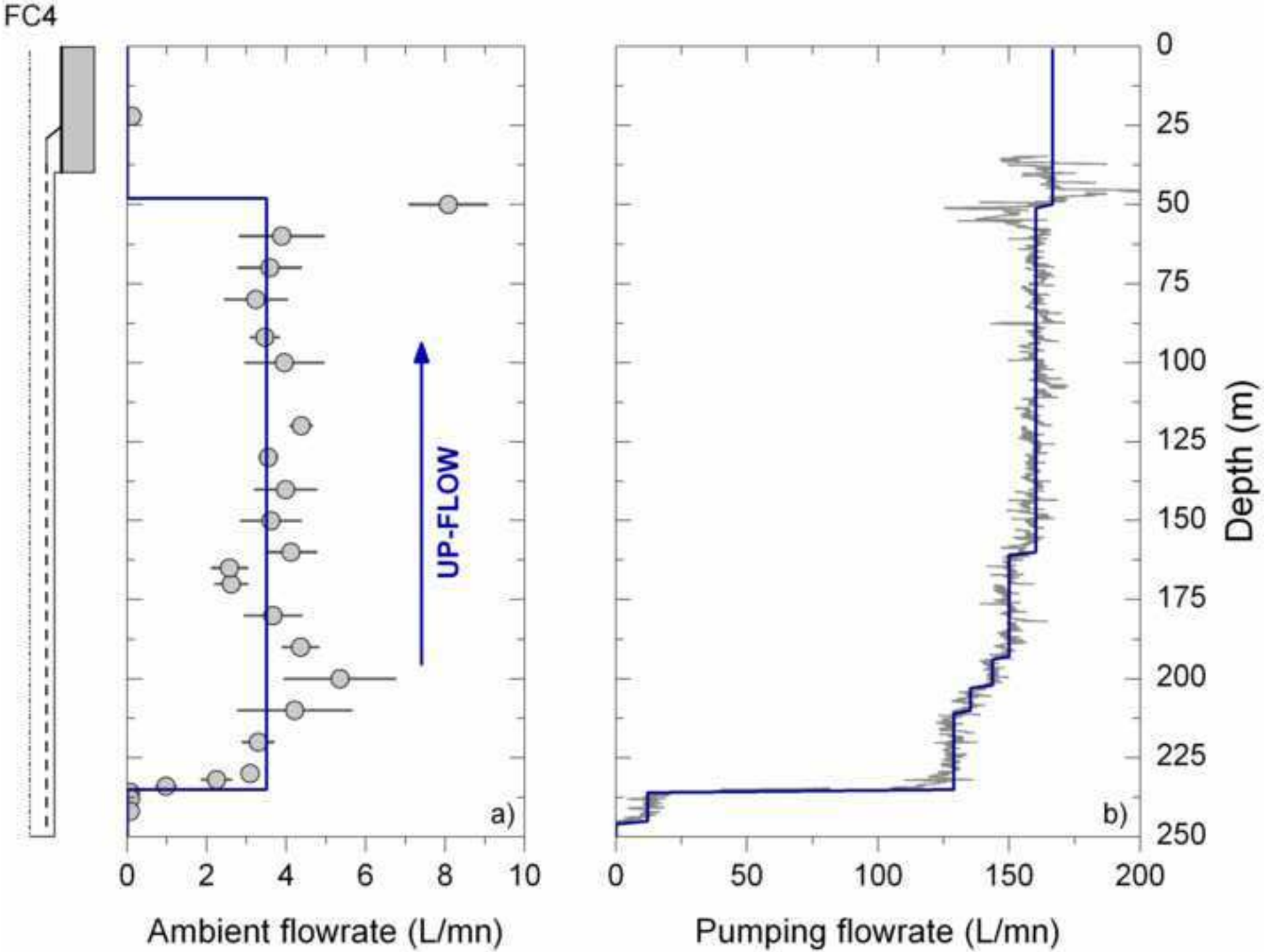

FIG5.tif

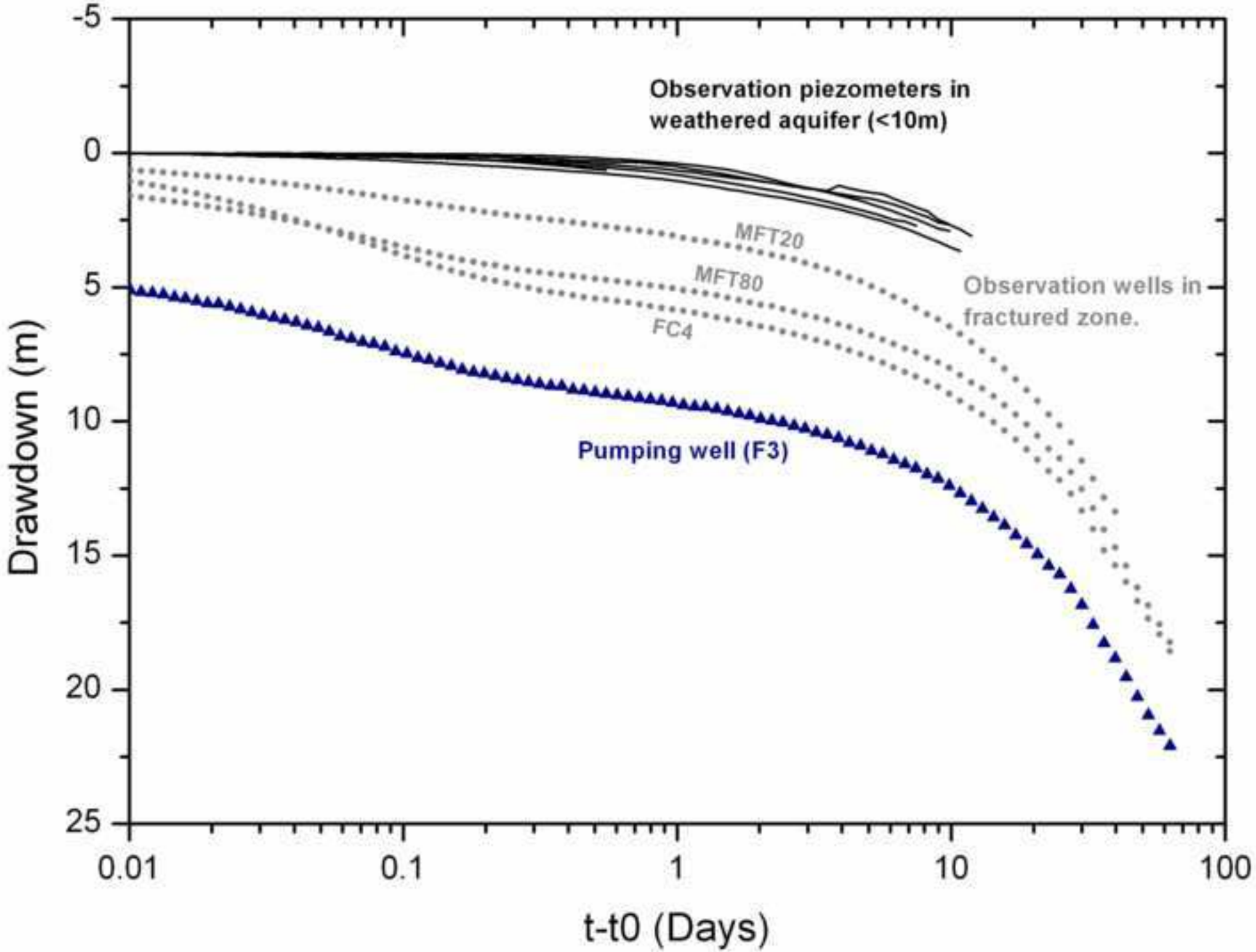

Figure

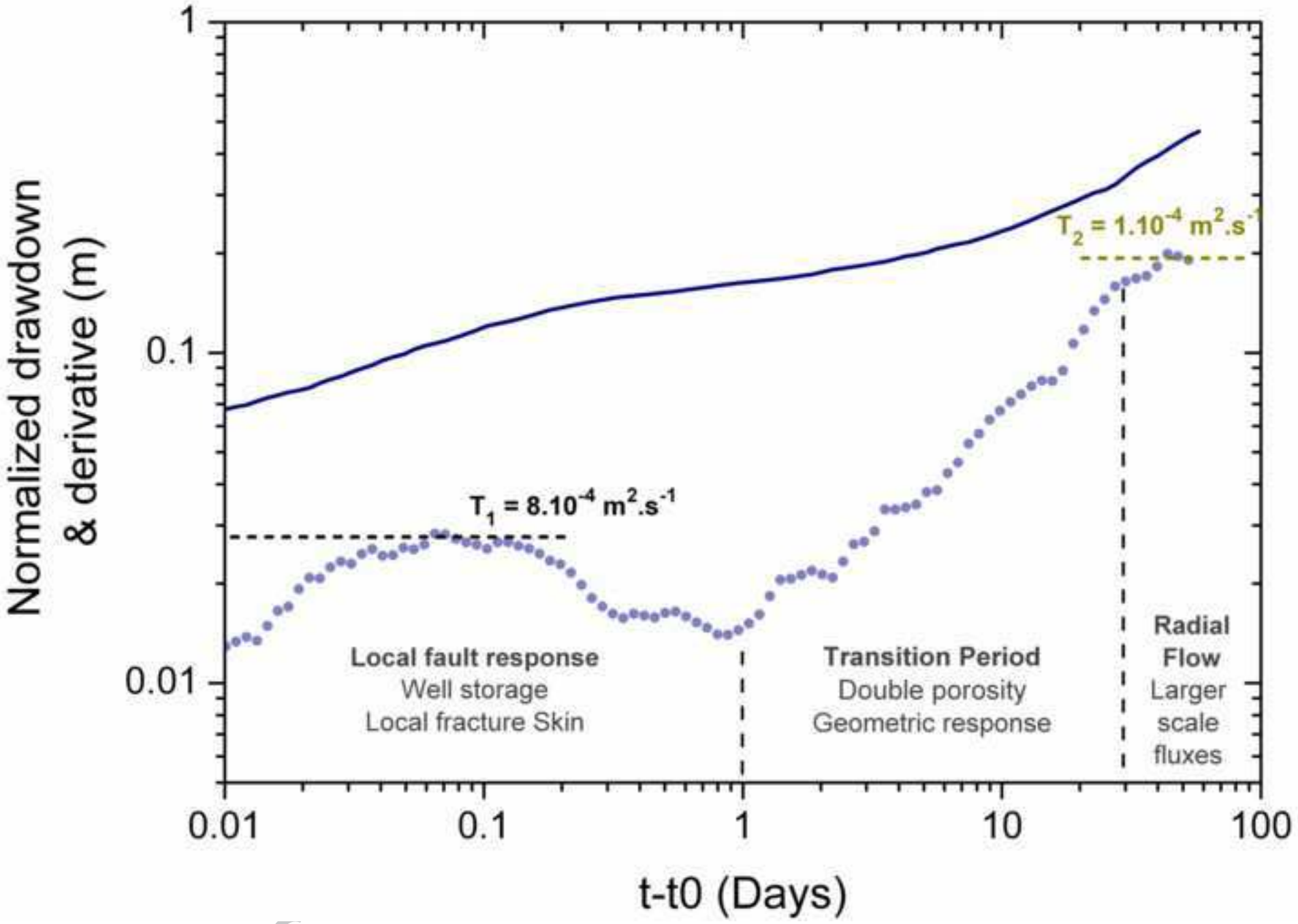

Figure

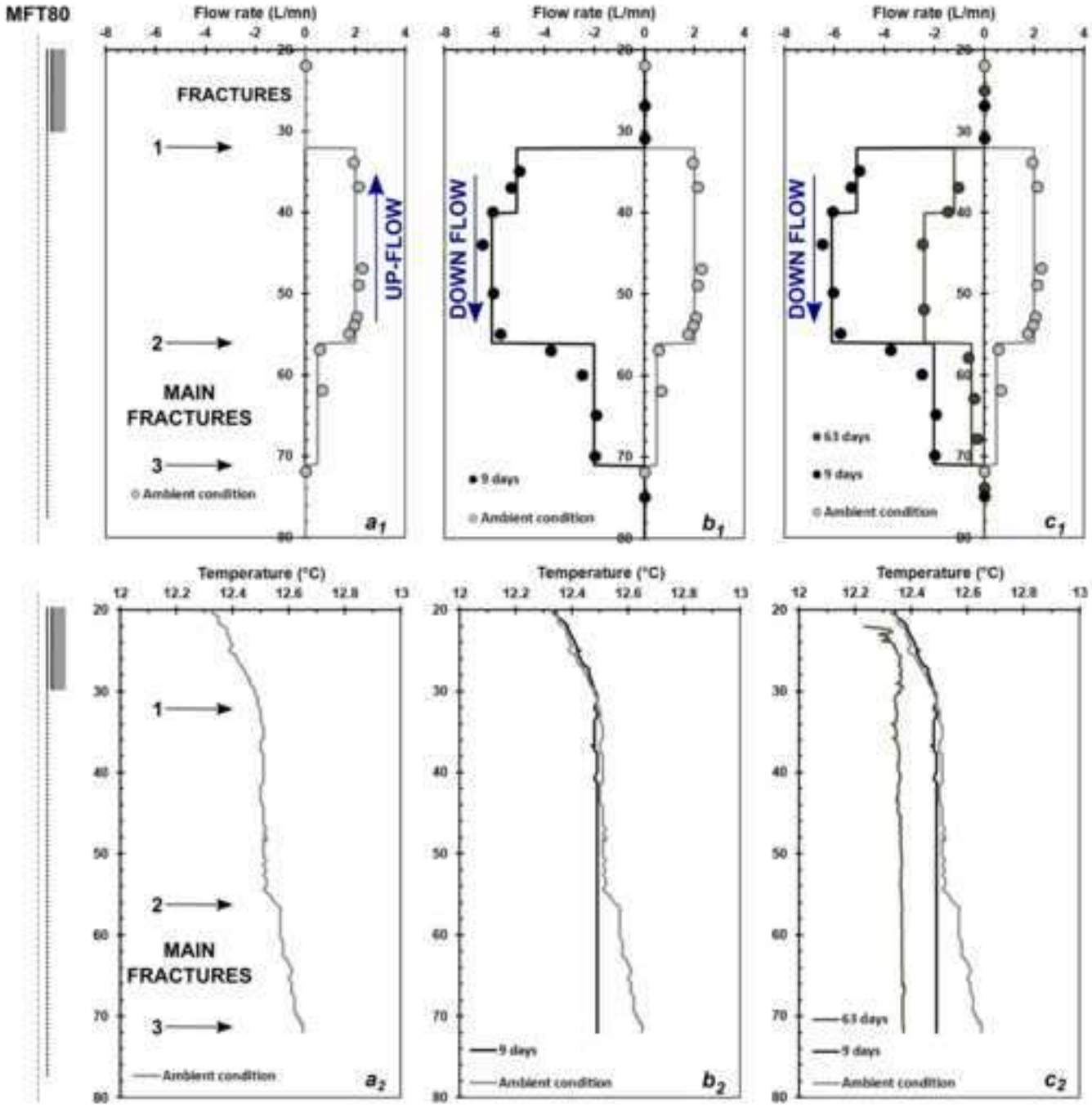

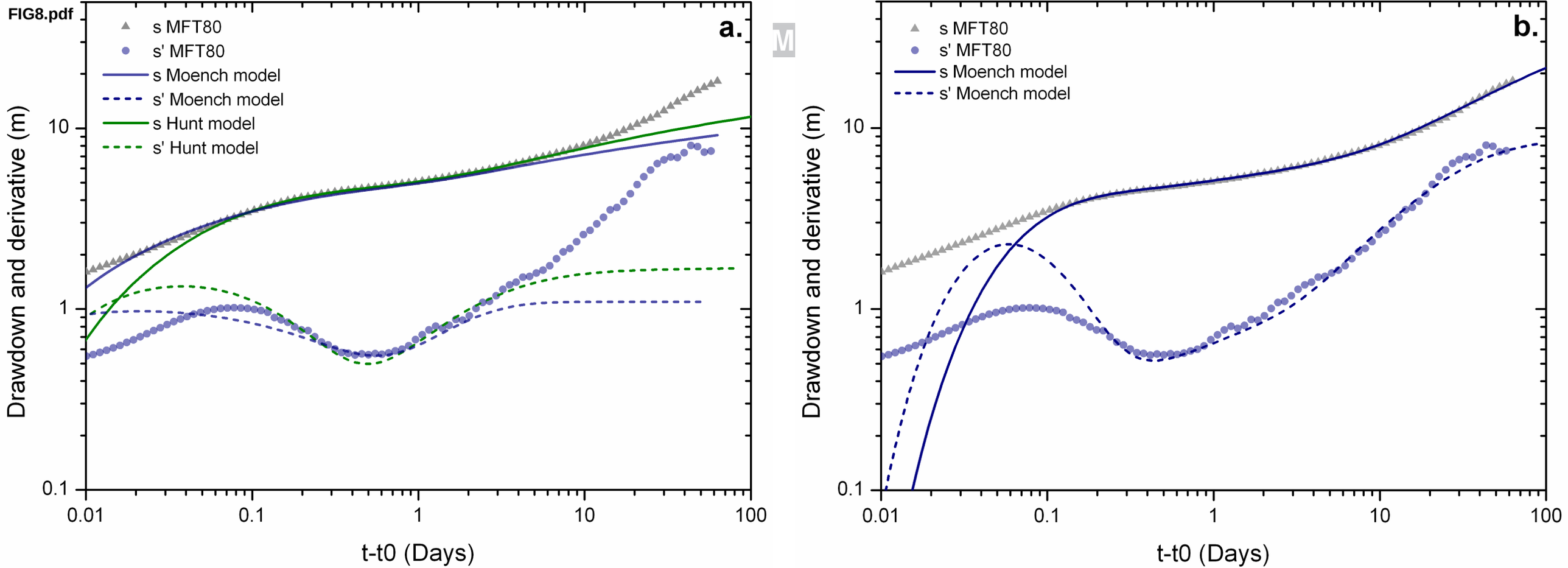
FIG8.pdf
a.
s MFT80
s' MFT80
s Moench model
s' Moench model
s Hunt model
s' Hunt model
Drawdown and derivative (m)
t-t0 (Days)
0.1
1
10
0.01
0.1
1
10
100
b.
s MFT80
s' MFT80
s Moench model
s' Moench model
Drawdown and derivative (m)
t-t0 (Days)

FIG9.tif

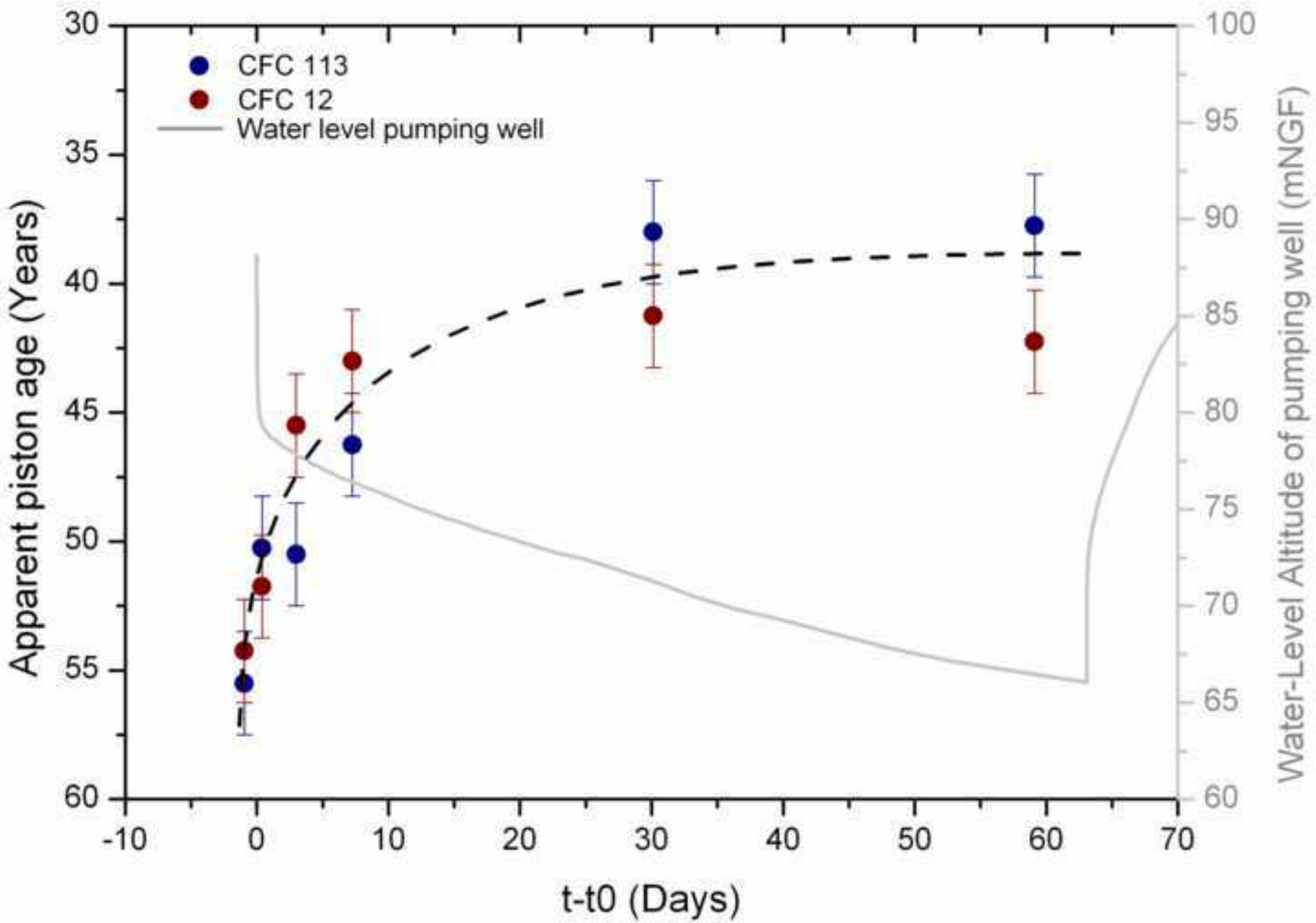

Figure

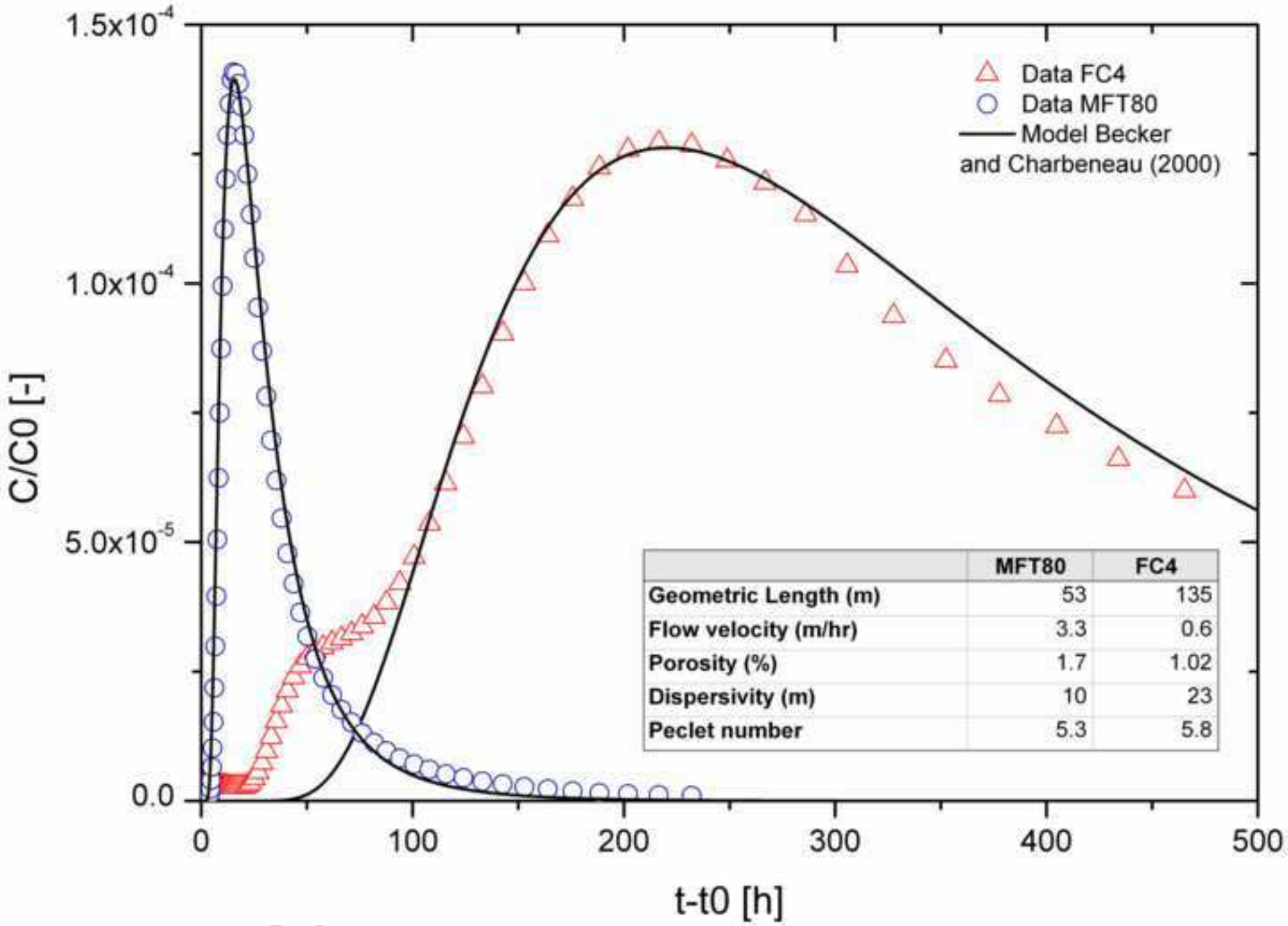

	MFT80	FC4
Geometric Length (m)	53	135
Flow velocity (m/hr)	3.3	0.6
Porosity (%)	1.7	1.02
Dispersivity (m)	10	23
Peclet number	5.3	5.8

Figure

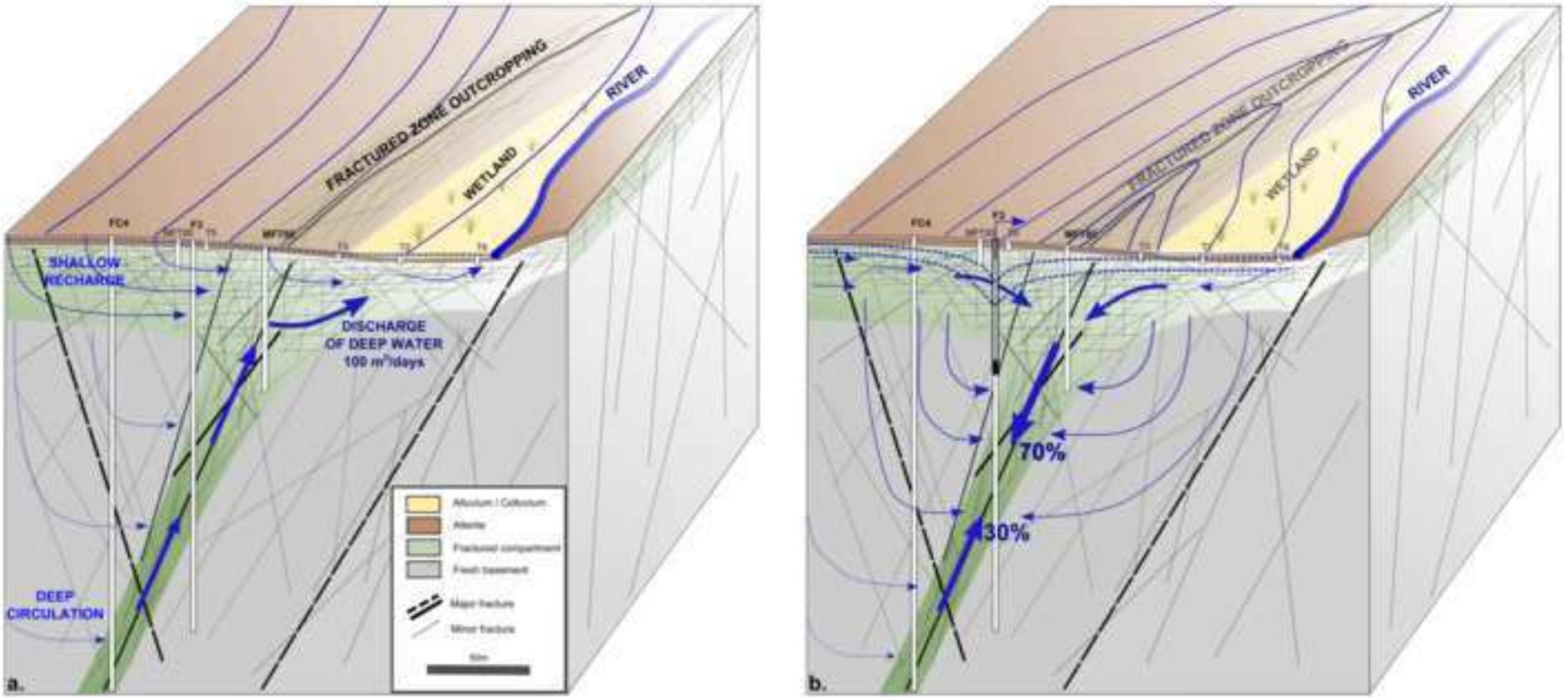

TABLE1.xls

Well	X (LAMB93)	Y (LAMB93)	Z (a.s.l.)	Depth (m)	Geology	Slotted zone (m)	Main fracture depth (m)
F3	376280	6822515	93.53	216	Brioverian bed rock	30 to 216	110; 135 ;160; 169; 180; 192
FC4	376252	6822521	95.1	250	Brioverian bed rock	40 to 250	160; 204; 235
MFT20	376286	6822500	93.68	20	Brioverian bed rock	10 to 20	-
MFT80	376305	6822511	91.14	80	Brioverian bed rock	30 to 80	52; 69
T1	376350	6822537	88.22	6	Alluvial deposits (wetland)	1 to 6	-
T2	376353	6822504	88.27	8	Alluvial deposits (wetland)	2 to 6	-
T3	376329	6822490	89.57	6	Alterites	3 to 6	-
T4	376255	6822496	95.55	8	Alterites	4 to 8	-
T5	376294	6822485	93.54	7	Alterites	4 to 7	-
T6	376314	6822530	89.63	7	Alterites	2 to 6.5	-
T7	376273	6822531	93.02	9	Alterites	5 to 9	-
T8	376389	6822521	88.06	3	Alluvial deposits (wetland)	0.5 to 3	-

TABLE2.xls

Well	Depth of fault zone (m)	Ambient Flowrate (L/mn)	Total transmissivity (m^2/s)	Fractured zone transmissivity (m^2/s)	Part of total productivity
FC4	235	3.5	$1.3x10^{-3}$	$9.8x10^{-4}$	75%
F3	90-116	3.5	$1.8x10^{-3}$	$8.8x10^{-4}$	50%
MFT80	48-53	2	$7.9x10^{-4}$	$5.9x10^{-4}$	75%

TABLE3.xls

Well	SF6 (pptv)	CFC-12 (pptv)	CFC-11 (pptv)	CFC-113 (pptv)
F3	0	50.13	6.03	14.47
FC4	0	19.85	5.83	31.04
MFT20	0.87	48.29	6.64	21.48
MFT80	0.5	52.93	5.11	24.22
T's (mean)	2.79	458.79	271.52	56.66

TABLE4.xls

Wells	Analytical models	Fault aquifer		Blocks parameters		Superficial aquifer			Error
		T (m²/s)	S (dless)	Kb (m/s)	Sb (1/m)	T0 (m²/s)	Sy (dless)	Kv (m/s)	*RMSE [m]*
F3	Moench early time	7.00E-04	-	2.47E-08	2.62E-04	-	-	-	*0.98*
	Hunt early time	4.79E-04	-	-	-	8.13E-05	-	-	*0.55*
	Moench global	**1.05E-04**	**7.00E-03**	**-**	**-**	**-**	**-**	**-**	***0.95***
MFT80	Moench early time	7.38E-04	7.00E-04	1.34E-09	1.15E-05	-	-	-	*0.59*
	Hunt early time	4.84E-04	1.80E-03	-	-	8.10E-05	0.02	1.09E-07	*0.37*
	Moench global	**9.03E-05**	**1.75E-03**	**1.28E-08**	**1.18E-03**	**-**	**-**	**-**	***0.56***
FC4	Moench early time	6.25E-04	8.40E-04	8.47E-10	9.84E-06	-	-	-	*0.93*
	Hunt early time	3.87E-04	1.61E-03	-	-	6.94E-05	0.02	8.00E-08	*0.21*
	Moench global	**1.13E-04**	**1.61E-03**	**8.15E-09**	**6.53E-04**	**-**	**-**	**-**	***0.57***
MFT20	Moench early time	6.02E-04	1.05E-02	3.35E-08	2.62E-04	-	-	-	*0.69*
	Hunt early time	7.27E-04	1.17E-02	-	-	5.79E-05	0.05	8.04E-07	*0.19*
	Moench global	**9.78E-05**	**7.00E-03**	**6.33E-08**	**3.07E-03**	**-**	**-**	**-**	***0.57***

1 We propose hydrogeological conceptual model of fault aquifer in crystalline basement.

2 We characterize interactions between a fault aquifer and surrounding compartments.

3 Sub-vertical fault resource is strongly dependent on superficial aquifer storage.

4 We estimate groundwater resource availability.

FIG_abstract.jpg